A Digital Workflow for the Design and Manufacturing of 3D Printed Concrete Bridges in a Circular Economy:

Structural Design Considerations for Pre-Stressed Beams and Dry Connections

于榕

Rong Yu

EINDHOVEN UNIVERSITY OF TECHNOLOGY

Stan Ackermans Institute

SMART BUILDINGS & CITIES

A Digital Workflow for the Design and Manufacturing of 3D Printed Concrete Bridges in a Circular Economy: Structural Design Considerations for Pre-Stressed Beams and Dry Connections

By

Rong Yu

A thesis submitted in partial fulfillment of the requirements for the degree of Professional Doctorate of Engineering

The design described in this thesis has been carried out in accordance with the TU/e Code of Scientific Conduct

Rob Wolfs & Theo Salet, university coach

Eize Drenth & Johan de Boon, company coach

Eindhoven, the Netherlands

October, 2022

This thesis has been established in collaboration with

Thesis Evaluation Committee

Scientific supervisor	Dr. Ir. Rob Wolfs	Eindhoven University of Technology
Scientific supervisor	Prof. Dr. Ir. Theo Salet	Eindhoven University of Technology
Company representative	Ir. Johan de Boon	Rijkswaterstaat
First independent member	Ir. Chris van der Ploeg	ABT
Second independent member	Dr. Katrin Schollbach	Eindhoven University of Technology
Chari of the committee	Dr. Ir. Astrid Kemperman	Eindhoven University of Technology

Acknowledgement

Through this 2-years project, I experienced a lot and grew a lot. I would like to appreciate all the people who supported me and helped me through this journey.

My first sincerest thank is to my scientific supervisor Rob Wolfs, who guided me to the 3D concrete printing world and showed me the excitement of digital manufacturing. I have learned a lot from his scientific thinking, writing and planning abilities. Rob, thank you for all the helps and I'll never forget the jokes you made. I am also grateful for the support and kindness I received from my scientific supervisor Theo Salet. He inspired me deeply with his enthusiasm for improving the industry. Thank you, Theo, for all the open conversations and your smile.

I would like to thank my company supervisors Eize Drenth and Johan de Boon, for their guidance, suggestions and industrial perspectives which help me to improve this project.

In addition, I would like to show my appreciation to the SBC management team: Astrid Kemperman, Lada Hensen Centnerová, Francien Clijsters and Vincent Merk, who are always considerate and willing to help. I would like to thank Chris van der Ploeg(ABT) and Katrin Schollbach, for being members of my evaluation committee and reading my report. I would also like to thank Volker Ruitinga(Vertico) and the people in Vertico, for helping us to produce our designed prototype.

Furthermore, I would like to thank all my colleagues, for providing me with such a warm, united and friendly working environment. To all the 9th-floor pals: it's my great pleasure to meet you all and I'll never forget the time with you. I would like to thank everyone in the lab, for helping me with experiments and sharing coffee and cakes. A great appreciation for Matthew Ferguson, who is my closest teammate for the past 2-years. Thank you, Matthew, it's great to have you as my teammate, especially in the lab.

I would like to express my appreciation to all my friends, for their care and support no matter how far between us. Special thanks to Xin Liu, Yucheng Liao, Flora, Yan Li and Ting Li, thank you for all the love and accompany, the time with you brightened my life.

The essential acknowledgement to my family, for their understanding and emotional support. I would like to give the most important appreciation to my partner Yue Zhang and my parents Linhai Yu and Haiyan Peng, thank you for your endless love and support, I love you all!

<div align="right">

Rong Yu
Maastricht, The Netherlands, Early Autumn, 2022

</div>

Abstract

Facing the environmental and social challenges of the construction industry, this design project aims to improve the productivity and sustainability of the design and manufacturing process. Considering the requirements from Rijkswaterstaat, an integrated digital workflow for post-tensioned 3D concrete printed bridge structures is presented. This project focuses on the development of an embedded structural design tool and dry connection design within this digital workflow, to provide users with real-time simplified structural feedback. The structural design is based on assumption in material and structural behaviour, thus experimental and numerical work has been performed as validation. The dry connection concept consists of the design for interlocking shapes and the design of interlayer materials. The dry connection prototype has been designed and validated experimentally. Based on these design works, the application possibilities of the structural design tool and dry connection concepts will be presented. The knowledge dissemination related to this project will be elaborated on as well. Finally, conclusions and recommendations for future developments of digital design and manufacturing 3D concrete printed bridges will be presented.

Table of Contents

Chapter 1. Introduction

This design project is part of the project named A Digital Workflow for the Design and Manufacturing of 3D Printed Concrete Bridges in a Circular Economy enabled by Rijkswaterstaat, which is a joint effort between two EngD candidates: Matthew Ferguson (focusing on a digital design tool) and Rong Yu (this report). Firstly , the background of this project will be introduced, including its relevance for the current status of the architecture, engineering and construction (AEC) industry , the requirements from Rijkswaterstaat, and the introduction of 3D Concrete Printing (3DCP) as the main technology in this project. The challenges in the current state of the art of the printing technology will be explained, which drives the ambitions of this design project. Finally, an   overview of this project will be presented, including its goals, deliverables, and the general design methodology, along with the report outline.
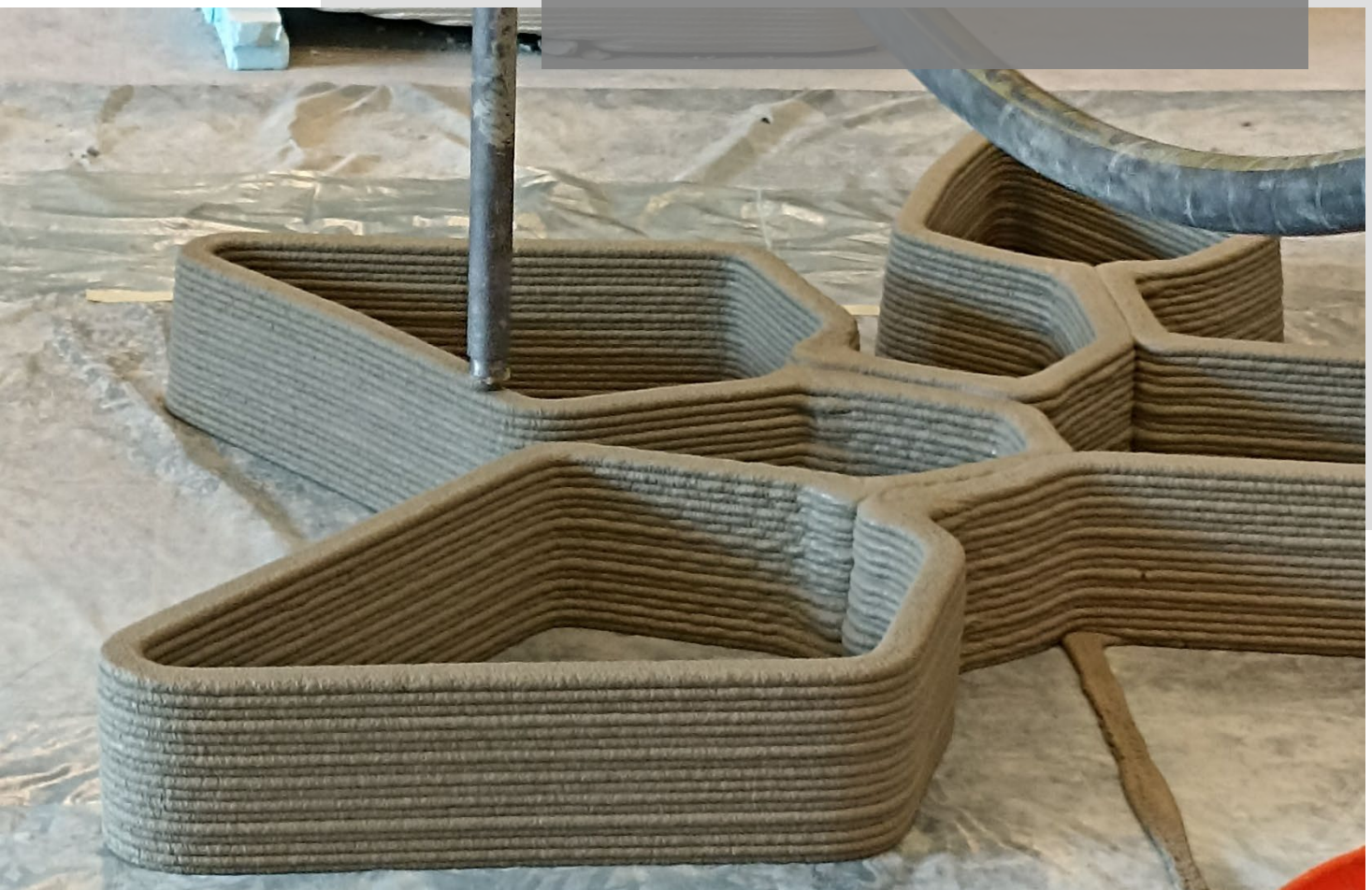
1.1 Background

The growing housing demand and the pressure from climate change lead to major problems in the current AEC industry: productivity is too low and environmental impact is too high. The labor shortage, has been existing for several years and the pandemic situation has worsened the problem. Globally, the growth of labor-productivity in construction sector was extremely slow comparing to the overall productivity increase over the past two decades. [1] Companies and organizations start shifting to digital collaborations dure to the increasing remote working situation at post-covid period. [2] It accelerate the requirement growth of new skills and technology which can improve productivity in construction industry. [3] Beside the low productivity, the sustainability in construction sector is also poor. Globally, nearly 40% of total carbon emissions and over 30% of extraction of natural resources are responsible by building and construction sector. [4][5] More than one third of the total waste generation is produced by construction sector in EU [6], 41% in the Netherlands [7], which are significantly triggered by the overlook of the treatment for buildings or infrastructures reaching the end of its service life. According to the National Waste Management Plan and Circular Economy ambitions, it is urgent to create a more sustainable solutions in construction industry. [8][9]

With the focus on infrastructure, especially on bridges, Rijkswaterstaat faces achallenge regarding their portfolio of bridges. The infrastructure built in the 1960s are ageing and suffering from fatigue due to the increasing traffic load. [10] This requires repair or replacement of these existing structures, reaching the end of their service life. Combined with the mentioned challenges in AEC industry, Rijkswaterstaat requires an innovative solution which boosts productivity and sustainability, and includes circular management, with consideration of its after-service use.

The innovation in 3D Concrete Printing technology is an excellent method to address both productivity and sustainability. Benefiting from a robotized manufacturing process, the 3DCP method can work without pause for a more efficient construction process under the supervision of a smaller working team. Concrete printing also doesn't need to build up scaffold and formwork so it saves time and material. Because of the form freedom provided by 3DCP, it is possible to optimize material use so that the total amount of material, and its carbon footprint, can be reduced. Therefore, the 3DCP process reduces labour, construction time, material and cost at the same time, and thus has the potetialy of a more productive and sustainable manufacturing method.

1.2 Problem statement

However, the 3DCP technology is still under development, and faces various challenges. One of the most important obstacles comes from the isolated design process. Currently, most 3DCP projects are generated from specific designs, under particular requirements for that project. The design-manufacturing process is therefore a one-off solution. Besides, the relevant design rules and standards(such as Eurocode) are still lacking for 3DCP, as a result of which every project requires extensive testing and analysis. This can be observed, for instance, from the design and testing of the 3D printed bridge projects in both Gemert and Nijmegen, in the Netherlands. In these projects a bridge prototype was printed and tested in the lab to prove its structural safety, followed by a non-destructive in-situ test. [11][12] These tests consumes time and labour, especially when repeated for each specific design. In addition, both bridges had glued connections between their segments, which minimizes possibilities for reuse after its service life.

(a)   *(b)*

Figure 1-1: The scale model in 4-point bending test set-up(a) and the completed bridge at the opening of Gemert 3DCP bridge(b), as described in [11].

(a)   *(b)*

Figure 1-2: The setup of the structural mock-up test of Nijmegen 3DCP bridge(a) and the assembly of final bridge on location(b), as described in [12]*.*

To addres these problems, the 3DCP process should not focus on one particular design, but rather be able to generate multiple design solutions based on different conditions. This resulted in the project ambition to develop a digital workflow from design to manufacturing, which should be able generate a large set of outputs, faciliting circularity (potential re-use). This digital workflow will include design aspects and manufacturing constraints to satisfy different design and production requirements, as well as structural design aspects to eliminate extensive experimental tests in the lab. The design aspects and manufacturing constraints in the digital workflow will be introduced by Matthew Ferguson's EngD report, while this report will focus on the structural design aspects.

1.3 Project overview

1.3.1 Project goals and deliverables

Facing the challenges from the industry and requirements from Rijkswaterstaat, a digital workflow will be generated with integrated design and manufacturing process for 3DCP structures. The goals of this project can be described as:

Productivity
This digital workflow will provide a more productive design and manufacture process of 3DCP bridge(beam) structures as it requires less human labour for manufacturing and it can generate various design options rather than one-off process. It also allows the users to assess the feasibility of the designs from a structural and fabrication perspective so that the design process can be more efficient.

Sustainability
The sustainable solutions such as material optimizations during design phase, or reusable structure after its service life etc, should be involved in this digital workflow, from the circular economy perspective. This digital workflow will enable material optimizations by introducing structural feedback in the design phase and realize the results with 3D printing manufacturing technology. The demounatble connections will be involved as well to allow reusability.

With an emphasize on prestressed 3DCP bridge(beam) structures, which consist of multiple elements, this project will focus on the structural design consideration and dry connection designs. Several project outcomes will be delivered:

- **Structural design tool**

The structural design tool aims at getting structural feedback for the users to make choices, not only from an aesthetic perspective with manufacturing constraints, but also from a material optimization view with the structural approach. Therefore, the users can generate various feasible outputs from this tool and it can eventually lead to the reduction of experimental validation. To realize this goal, the structural design tool suggests prestressing locations and provide indications of the structural performance of the designed shape at the cross-sectional level. This structural indication allows the users to optimize the material use so that they can generate more sustainable deliverables. The involved prestress location aims to guide the application of prestressing force for positive structural impact(compression for concrete).

- **Dry connection prototype**

This project explored the potential for demountable(dry) connections, with the consideration of the reuse of the structures after their service life. It helps to reduce the waste from demolition and also provides the possibility of reusable temporary structures. A prototype of 3DCP dry connections(including the design of interlocking shape and interlayer material) will be designed and validated, as the suggestions to the user for circular application of bridge(beam) structure.

- **Knowledge dissemination**

Disseminate the possibility and prospect of digital workflow with embedded structural design tool for 3DCP structures. Publicize the potential of dry connections for 3DCP structures from a circular perspective.

An overview of this project is demonstrated in the framework below:
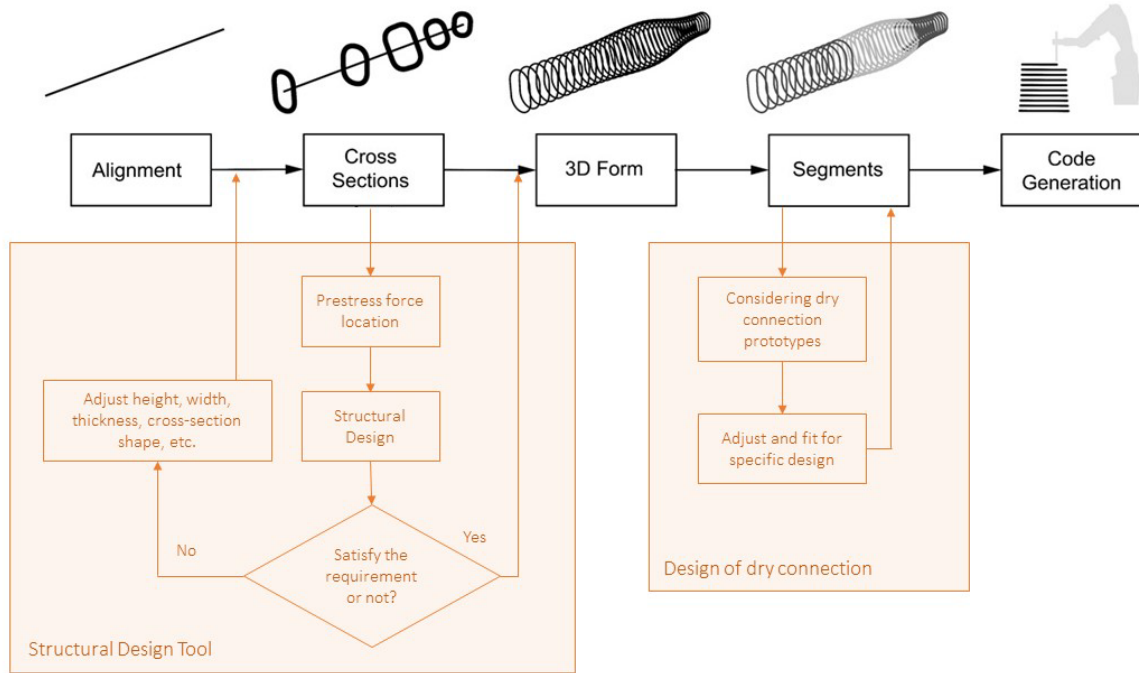
Figure 1-3: The project overview.

1.3.2 Design methodology

- **Structural design tool**

The structural design tool is created based on the design criteria addressed in chapter 2. It is established in the same parametric environment as the digital workflow. The structural calculations are obtained by embendded python code, with certain assumptions. A series of the experimental tests are implemented to validate the assumptions in the structural design tool. The numerical analysis is also involved to assist the experimental validation.

- **Dry connection prototypes**

To facilitate circularity, the dry connection is designed separately in interlocking shapes and interlayer materials, following the design criteria introduced in chapter 3. The numerical models will be established to explore the possible interlocking shapes. The limitation of digital manufacturing is also considered when designing interlocking shapes. The validation of the dry connection is obtained by an experimental test.

- **Knowledge dissemination**

The potential application of the structural design tool and dry connections will be explained through user stories in chapter 4. The knowledge dissemination can be obtained by attending conferences, showing physical beams designed through this digital workflow in exhibitions, and speading information in academia and industry, which will be explained in chapter 5.
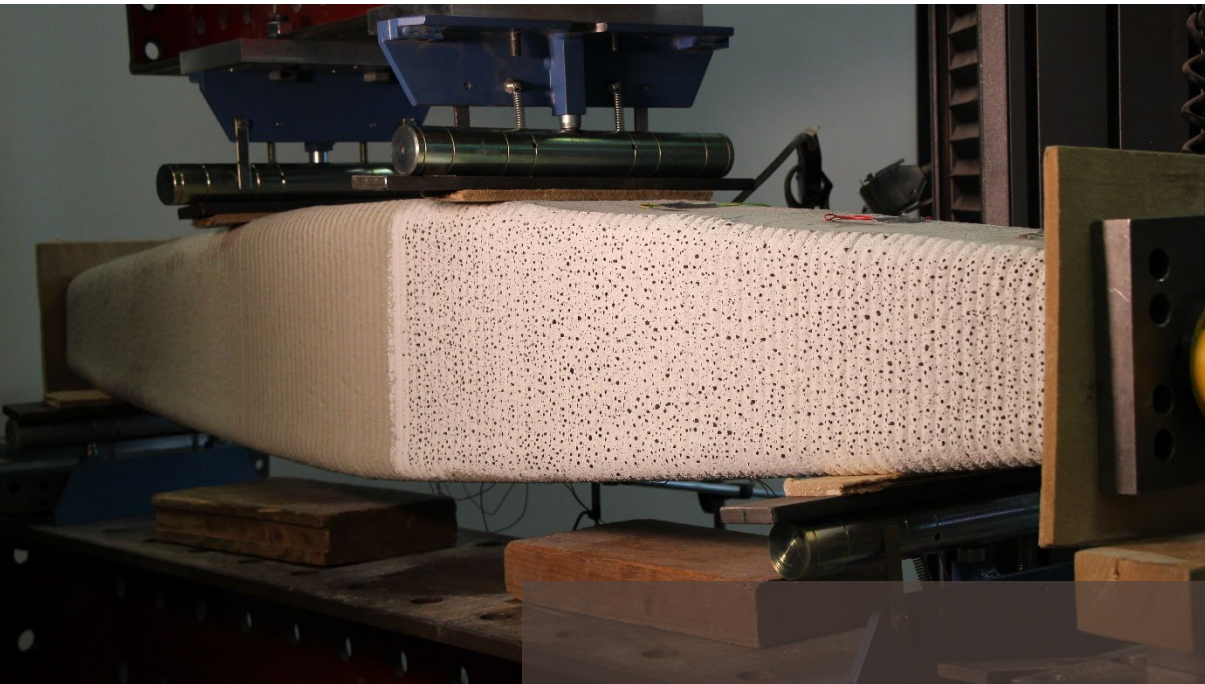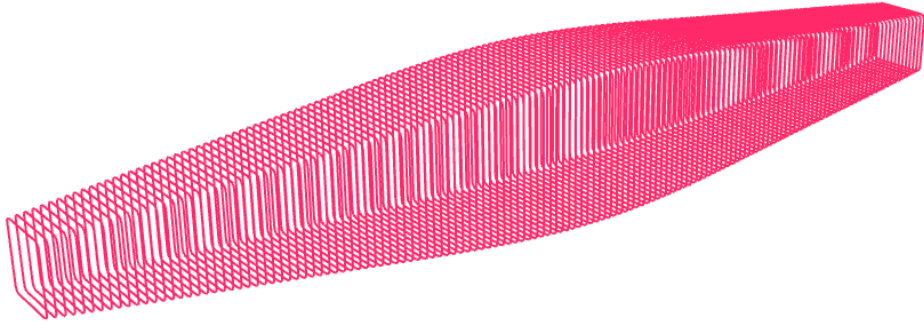
Chapter 2. Structural design tool

This chapter will discuss the development and validation of the structural design tool. The general design criteria will be elaborated to guide the design process, followed by the introduction of detailed design approach. To validate the design, a set of experimental tests and numerical models will be presented, as well as the relevant analysis and discussions. Finally, the assessment of this structural design tool will be illustrated assisted with the simplified user instruction.

2.1 Design criteria

Based on the ambitions mentioned in chapter 1, the design criteria of this structural design tool from users' perspective are listed below:
- **Real-time simplified structural indications**

This structural design tool will provide users possibilities to modify their design based on structural evaluations in early phase. It is necessary that this evaluation results is easy accessed and fast given, which claims for a clear input requirement and a rapid calculation process. The structural indication should also have a promising accuracy within certain amount of tolerance. Therefore, the selection of calculation theory and relevant assumptions is very important.
- **Clear visualization for material use**

Considering the function of optimized material use integrated in the structural design tool, the structural design tool should deliver clear indications for the material efficiency. The user should have a clear answer of where to remove some material and where is not sufficient in their design.
- **Clear visualization for possible prestressing locations**

The range of prestress locations should be provided to ensure the positive impact from prestressing force on structural performance under bending. Through visualize the prestressing locations can also avoid intersection between prestress cable and the structure.

2.2 Design methodology

2.2.1 Design approach of structural design tool

Following the ambitions and design criteria, the structural design tool is generated in parallel to the design tool within the same environment(Rhino & Grasshopper environment). Thus the users can receive immediate feedback while adjusting their design. This fully parametric environment also benefits for directly using geometric dimensions from the design as the input for structural calculation, leading to an easier and more accurate structural evaluation.

Considering the concrete material behaviour(poor performance in tension) and focusing on bridge structures(which can be simplified as beams), the structural design tool will focus on the bending beahviour of beams under vertical loading(external load and self-weight) and prestressing force. To reduce the calculation workload for a faster evaluation process, the structural calculation is applied to the cross-sectional level. A certain amount of cross-section along the beam is checked to ensure both the accuracy and efficiency of the results. To create a more user-friendly interface, the structural calculation is obtained by Python code which will run in background.

The structural evaluation is realized by comparing the total stress value under certain loading conditions with the concrete strength. Considering the weakness in tensile behaviour of concrete, there are 3 major stress requirements defined:
- The cross-sectional shear stress of the concrete structure should be in the range of tensile strength;
- The compressive stress in the concrete structure will not exceed its compressive strength;
- The tensile stress in the concrete structure should no more than its tensile strength.

Based on these criteria, the calculation is focused on the values of bending stress, compression stress and shear stress in the structure. The basic Euler–Bernoulli beam theory is adopted, with a simplified linear theory of elasticity. To simplify the calculation, several assumptions are applied before the calculation:

Material assumption:
- Linear material beahviour for the 3DCP structures
- Homogenous material.

Structural input assumption:
- The physical geometry is the same as the designed dimensions.

Loading scenario assumption:
- Simply supported beam
- Distributed vertical load and distributed prestressing system.
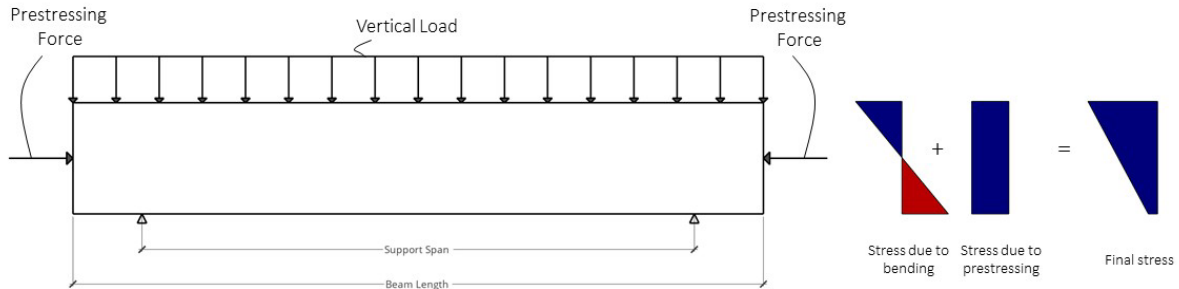- No impact from rotatory inertia.

Figure 2-1: The loading and support conditions of beam structure, with stress diagram.

On the basis of this theory and assumptions, the cross-sectional bending stress, compressive stress and shear stress will be calculated as the following equations [13]:

$$Bending\ stress = \frac{M_g}{w} + \frac{M_q}{w} - \frac{P}{A} - \frac{M_p}{w}$$

$$Compressive\ stress = \frac{M_g}{w} - \frac{P}{A} - \frac{M_p}{w}$$

$$Shear\ stress = \frac{(F_q + F_g) * S}{I * b}$$

Mg: the bending moment due to self-weight; Mq: the bending moment due to distributed load; Mp: the bending moment due to the eccentricity of prestress force; P: the prestress force; Fq: the shear force due to distributed load; Fg: the shear force due to self-weight; A: the cross-sectional area; w: the resisting moment to the bottom fibre; I: the moment of inertia;S: first moment of area; b: the width of cross section.

The bending moment and the shear force will be derived from the loading, according to the static beam equations. The supported span, beam length(alignment curve), and varying cross-sections and their locations along the span will be defined by the users. The cross-sectional properties will be calculated in Grasshopper, such as the cross-section height, width, area, resisting moment and moment of inertia etc. The parameters mentioned above, including the loading information and material properties, will be used as the input for the Python script(Appendix A) to derive and compare the stress based on these equations. The self-weight will be derived in Python script based on the designed shape and material density, such that it will change immediately with the adjustment of design. The calculations in Python script are established with the help of Sympy and Numpy library. The Python Remote plug-in is introduced for employing libraries in Grasshopper. Finally, the structural algorithm will provide visual feedback to the user regarding the stress level in comparison to predefined material characteristics. This allows the user to adapt, where applicable, cross-section shape, scale, or thickness, or adjust global features such as span length or support locations.
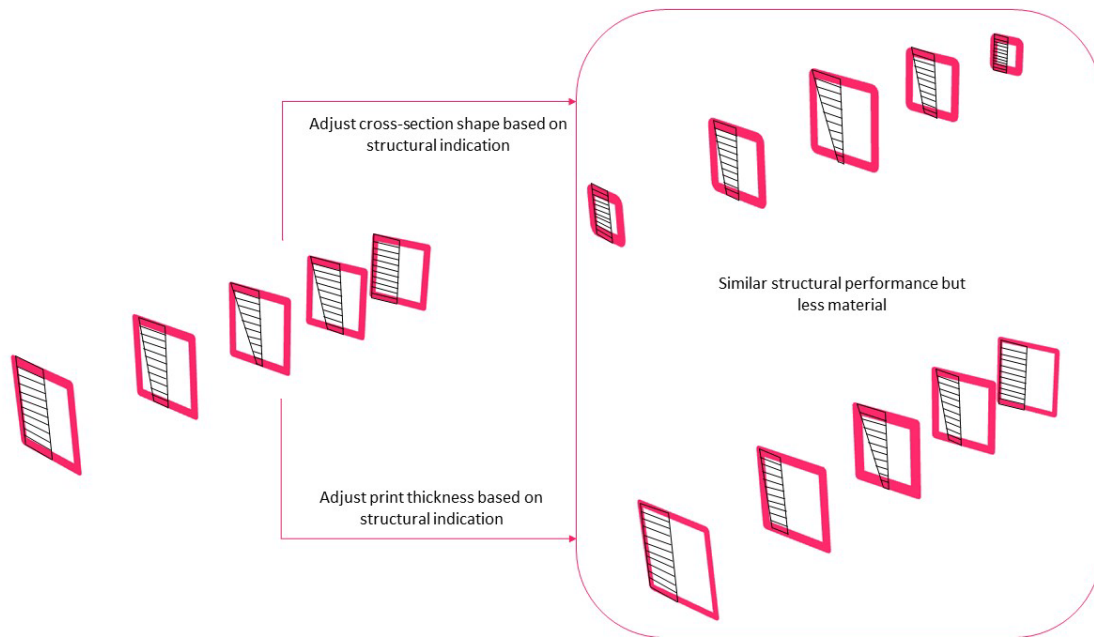
_____

Figure 2-2: The scheme of using structural design tool based on stress performance.

As mentioned, this structural evaluation results under the precondition of constant Young's modulus and uniformly distributed stresses, which is uncertain in the actual 3DCP structure. It is essential to validate this structural check, for clarifying the differences between theoretical calculation with the actual performance of 3DCP elements. The necessity of the design tool validation can be concluded as three aspects: the material influence, the bulk property difference impact and the geometric shape effect. [14] The uncertain material behaviour relates to the innovative manufacturing process. Unlike the isotropic structures produced by the traditional concrete casting method, the addictive manufacturing process generates concrete structures in layers, which leads to unknown influence factors in the stiffness of different directions to the interface. According to [15], the individual process parameters(such as interval time and curing conditions) are proven to influence the structural behaviour of the final product, nevertheless, it is difficult to control and predict. The bulk property of printed elements is very likely to differ from the designed dimensions. It can be influenced by pump pressure, nozzle height, nozzle speed etc, during the manufacturing process. The distinctions are even rising with the increasing freedom of the form. Last but not least, the geometric shape is usually presented as a complex structure, but the structural check is only based on 1D mechanical schemes(cross-sectional level). This complex geometric shape can introduce uncertainties in actual mechanical performances. For example, the stress distribution in thin shell concrete structures can not be confirmed as linear behaviour. Above all, it is mandatory to implement the validation of the design tool to investigate the gap between the design tool and the printed structure.

2.2.2 Design approach of prestressing location determination

The basic ambition of defining this prestressing location is to ensure the prestressing force applies compressive stress in the structure. In other words, tensile stress or torsional moment should not be created by this prestress application. By defining where the corresponding neutral axis is outside the cross-section, the collection of force centres will be found, known as the kern area of the cross-section.[16]

The kern area is formulated by the connection of core points derived from the corresponding neutral axis which is at the boundary of the cross-section. The position of each core point can be calculated based on the following equation:

$$\begin{bmatrix} e_y \\ e_z \end{bmatrix} = -\frac{1}{EA}\begin{bmatrix} EI_{yy} & EI_{yz} \\ EI_{zy} & EI_{zz} \end{bmatrix}\begin{bmatrix} 1/y_1 \\ 1/z_1 \end{bmatrix}$$

ey: the eccentricity in y-direction of the normal force; ez : the eccentricity in z-direction of the normal force; E: Young's modulus; A: cross-section area; Iyy & Izz: moment of inertia; Izy & Iyz: product of inertia; y1: the y value from the neutural axis intersects the y coordinate axes; z1: the z value from the neutural axis intersects the z coordinate axes.

Figure 2-3: The scheme of prestressing range.

Considering the assumptions in the design of the structural design tool, the torsional moment is eliminated and the material is homogeneous. Therefore, to simplify the calculation, 2 assumptions for the design of prestressing location are listed:

Assumptions:
- Homogeneous material in cross-section;
- Cross-section symmetric to z-axis to avoid torsional

As a consequence, the quantity of Young's modulus can be cancelled due to the constant value. The product of inertia can be removed because of the symmetrical cross-section. Based on this basic theory and assumptions, the calculation will be obtained by Python algorithm, which is working at background for a more tidy user interface. The determination process will be implemented at the cross-sectional level, starting with collecting critical points on the boundary of the cross-section. Afterwards, the list of coordinate values of these points, the cross-section area, the coordinate values of the neutral centre of the cross-section and the moment of inertia will be used as the input for the calculation. The Python script will generate the coordinate value for a set of core points, which will indicating the range of prestressing location. After the prestressing range defined, the user can adjust the eccentricity(distance between prestressing location and netural centre of the cross-section) as the input for satisfying structural check mention in chapter 2.2.1.

2.3 Design validation

2.3.1 Validation ambitions

In this project, experimental testing and numerical modelling are selected to validate the structural design tool. Three beams will be generated by the design tool, using its structural design functionalities,and will also be physically manufactured based on the the robotic manufacturing script generated from the tool, such that they could be used for experimental tests. With the aim of verifying the assumptions in the structural design tool, the experimental test targets the structural performance under vertical loading with constant prestressing system conditions. A 4-point bending test is selected due to the difficulties in applying evenly distributed vertical loads. The measurements focus both on global deflections and and local deformations/strains due to prestressing and bending. As a result, the material behaviour, stress distribution and geometrical dimensions can be compared and verified. In additiona to the experiments, numerical models are established with the designed geometry, such that

structural influence factors (such as prestressing eccentricity, unsymmetrical vertical load or different physical geometry) can be evaluated. The structural performance under ideal loading conditions can be derived from the numerical model to compare with the experimental results. The material assumptions and loading condition assumptions can be further validated.

2.3.2 Experimental validation

2.3.2.1 Experimental set-up

Two sets of three beams were manufactured and tested. Firstly, the beams were produced at TU/e in multiple elements and glued together for preliminary tests (discussed in Appendix B). Then, the same beams were produced in a monolithic version, to minimize the influence of (glued) connections, by the 3D printing company Vertico, which will be described here. Beam 1 is the basic shape formed with constant cross section area, thickness and outer geometry along the beam, while beam 2 and beam 3 is the variant from the basic shape. The shape of beam 2 is aligned with the bending moment distribution along the beam with a constant thickness. It has the same cross section geometry on the middle of the beam comparing to beam 1, but has smaller cross section area at the end of the beam. The beam 3 is also designed to fit the bending moment distribution but only through changing the thickness of cross section. The three beams are planned to be designed based on affordable strength suggested from the structural design tool. While due to the limitations of minimum print width, the designed affordable strength for beam 3 is slightly higher than the other beams. As the result, beam 1 and beam 2 have similar stiffness at the middle of the beam, and beam 3 have a higher stiffness for the middle cross-section. The calculation is under the assumptions of 30kN central applied prestress force, 45 MPa compression strength and 4 MPa tensile strength.
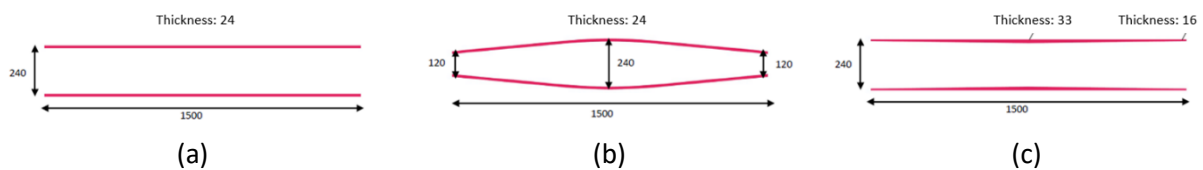

(a)   (b)   (c)

Figure 2-4: The geometry of beam 1(a), beam 2(b) and beam 3(c)

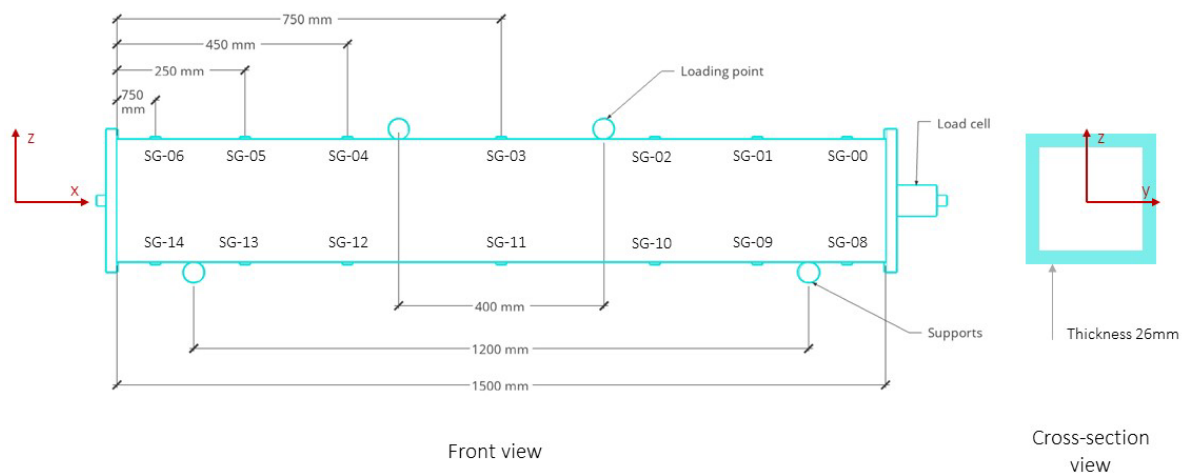Front view   Cross-section view

Figure 2-5 : The test setup scheme(beam 1 as the example).

The scheme of 4-point bending test set up, the location of strain gauges and the captured area of DIC camera is shown in figure 2-5. Except for the load cell and displacement-controlled loading machine to respectively record the prestress force and vertical load, there are Linear Variable Differential Transformer(LVDT) equipment to capture the displacement at the middle of the beam. The strain

gauges are distributed evenly on the top and bottom surface of the beam to collect the deformation during prestressing and loading. To capture the material deformation while loading, the 3D DIC measurement set-up is build up based on DANTEC Dynamics DIC system with the operation of the Istra4D software. In order to satisfy the best accuracy with bigger field of view, the half side surface of the beam is grinded and painted with white painter as observation aera. According to the requirement from this DIC system, the speckle size is defined to fulfill the requirement as 3 speckles in one pixel. This DIC measurement system aimed as capture the deformation on the side surface, to verify the linear behaviour from top to bottom surface of the beam.

The same test schedule is implemented to all of 3 beams, start from prestress force, which is applied manually through wrench and the strain is captured by DIC camera and strain gauges every increase of 3 kN. After the prestress stabilized, the loading system will grow up until 10kN with a speed of 0.25mm per min, following by a unloading with the same speed. Similarly, the process will be held under same condition up to the maximum load of 15kN and until break.
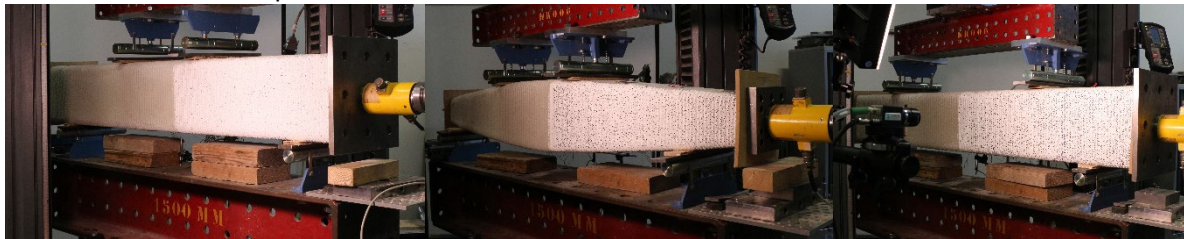
(a)   (b)   (c)

Figure 2-6 : The test setup of beam 1(a), beam 2(b) and beam 3(c).

## 2.3.2.2 Experimental results analysis
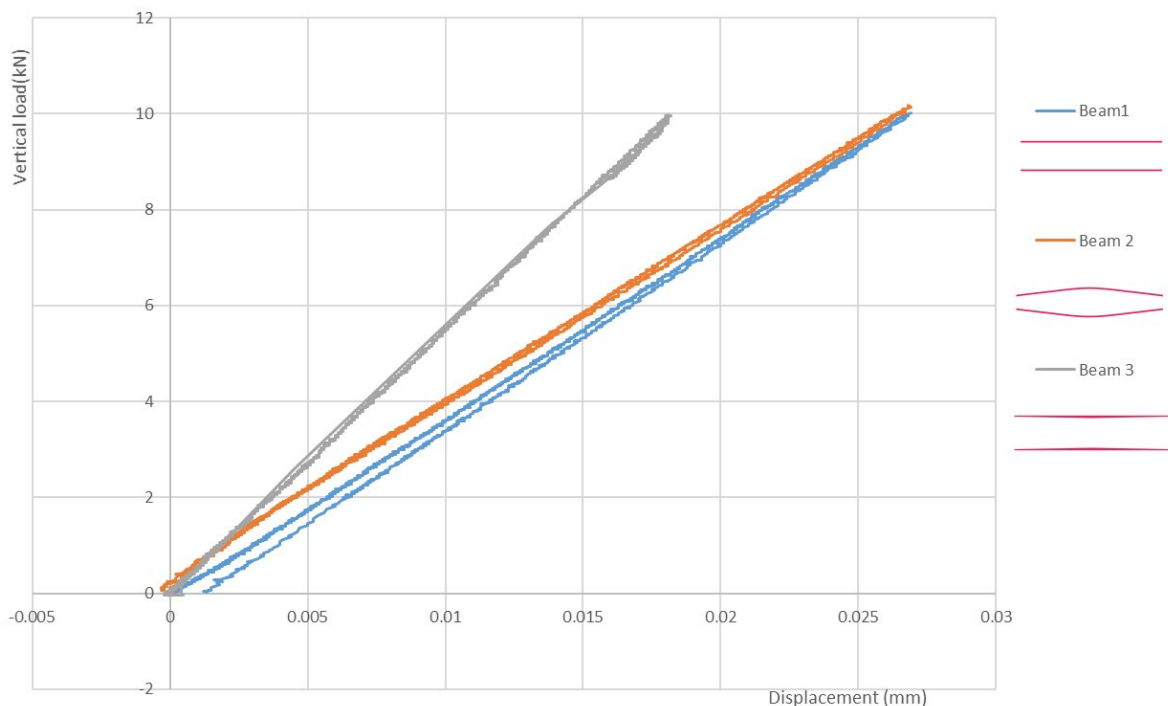
Chart 2-1 : The 10kN loading 4-point bending test of 3 beams.

As shown in chart 2-1, the straight lines for all of 3 beams under 10kN loading conditions proved the linear-elastic behavior as the evidence by the loading-unloading sequence. No damage or failure is

observed among 3 beams. The beam 1 and beam 2 shows a similar displacement, whereas beam 3 deforms less under the same loading condition. According to the designed dimensions, the beam 1 and beam 2 has the same stiffness at the middle of the beam, while beam 3 has a higher stiffness at the same location. Therefore, the displacement change under similar loading conditions of 3 beams is satisfied with the expectations. Since all beams use a different amount of material, one can compare the vertical load(kN) result in the same displacement(at 0.015mm displacement) to the total weight(kg) of each structure. This results in a weighted structural performance of 0.091 kN/kg, 0.133 kN/kg and 0.150 kN/kg for beam 1, 2and 3 respectively. Compared to the reference beam 1, beam 2 and beam 3 clearly shows a more efficient structural performance. It confirms the efficacy of shape optimization through structural design tool and 3DCP technology.

With the purpose of verifying the prestress distribution along the beam, the strains along the beam are collected by strain gauges while adding prestress force. The strain measurement is cleared to zero before adding prestress force to remove the influence from self-weight. In general, all of the strains present linear increasing as proof of the linear behaviour of the material under compression. Here the strain from the top to the bottom surface are assumed as linear, as straight lines in figure below. While this linear distribution can varies in thin wall structures due to the complex stress distribution in the cross-section. This situation is planed to be verified with DIC method, the result is however not valuable. The failure of strain collection through the DIC method can result from the poor quality of speckle patterns which is applied manually. The other reason possibly comes from the strain value being too small compared to the field of view, hence the result is easily influenced by the image noise. The strain condition under approximately 1.35MPa prestress for 3 beams is taken for analysis, as shown in figure 2-7.The strain at the bottom fibre is generally higher than the value at top surface for all beams, indicating an eccentricity of prestress locations to the minus z direction despite of the careful approach to apply it centric. The strain distribution due to prestressing in x direction is also not even, there are a slight concentration in the middle of beam 1, while more to the end of beam 2 and beam 3. Above all, the prestress distribution is not as assumed. Therefore, the design of the bulkhead is very important, which not only helps to address prestressing force in the desired location, but also helps to distribute prestress.
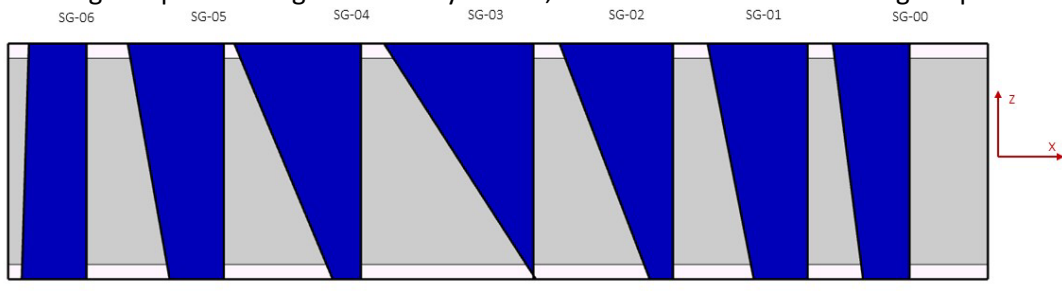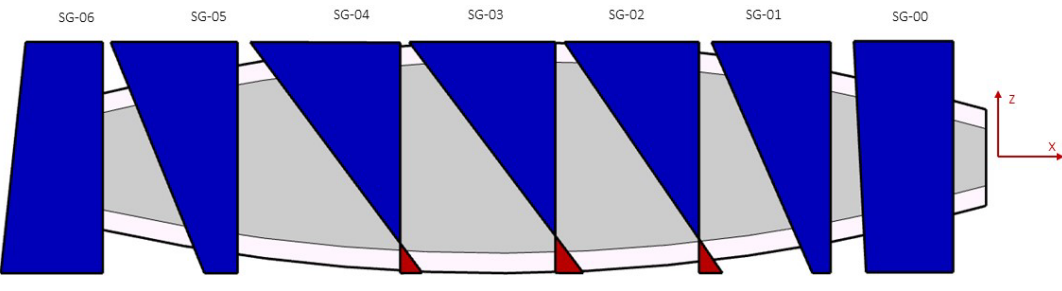

Beam 1

Beam 2
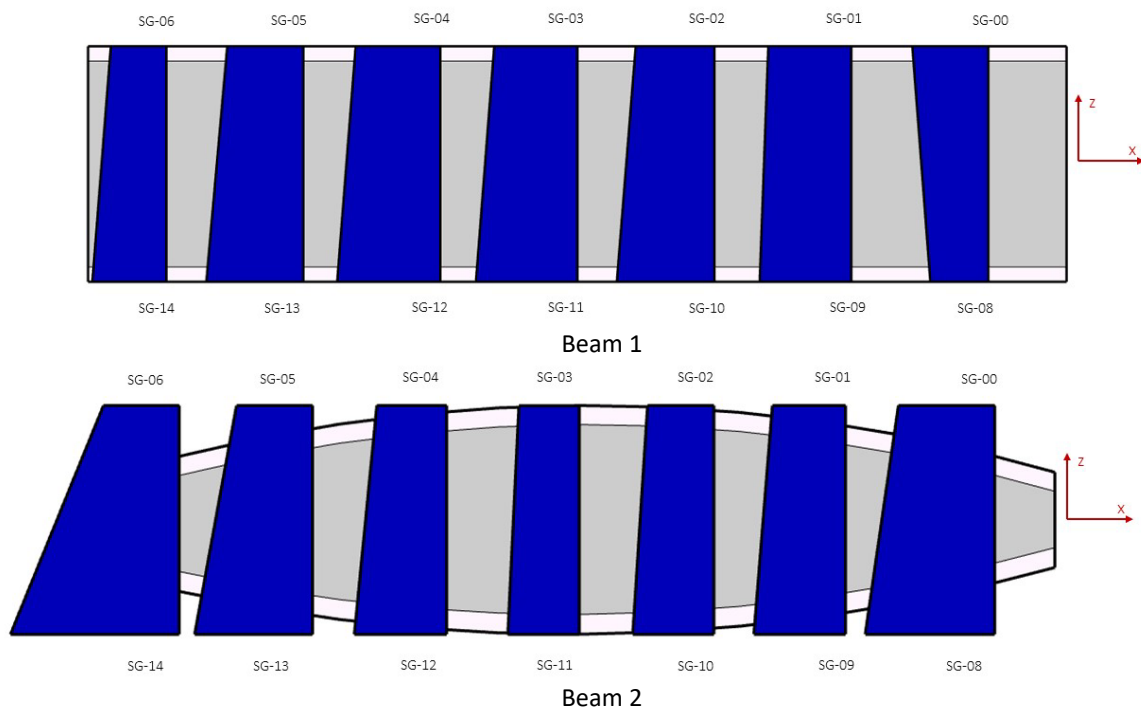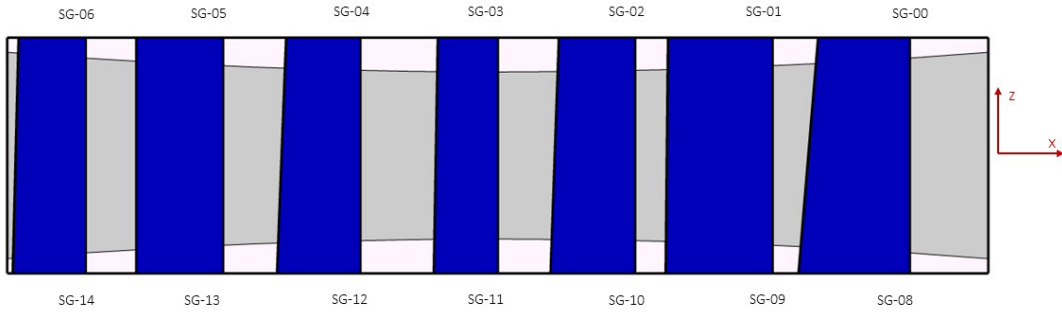
Beam 3

Figure 2-7 : The strain condition of 3 beams under around 1.35MPa prestress, blue area indicate strain due to compressive stress while red area indicate the strain due to tensile stress.

The diagram below presents the strain condition of 3 beams at around 10kN vertical bending load and around 1.35MPa horizontal prestress. Compare to the stress condition under pure horizontal prestressing, figure 2-8 shows obvious bending influence with the significant decrease of compressive stress or the appearance of bending stress on the bottom surface. In all three beams, the influence of bending stresses increases towards the middle of the span, which follows the bending moment distribution. Even though the strains at the bottom fibre in beam 2 show more bending deformation compared to the other beams, the difference is not dramatic. Overall, the stress condition of 3 beams under bending and prestressing are basically similar, which is conform to the design expectations.

Beam 1

Beam 2
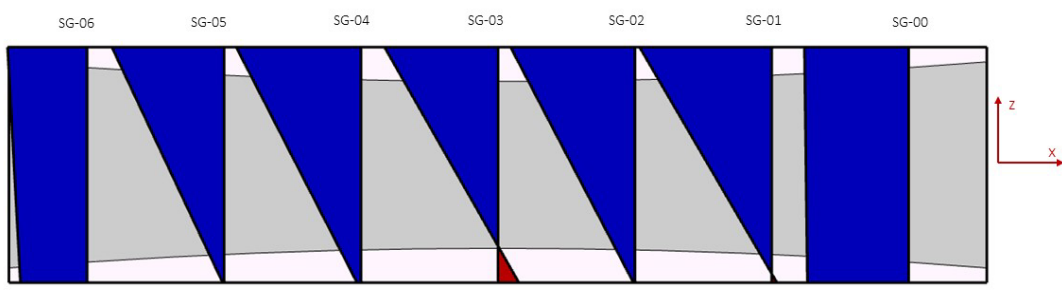
Beam 3

Figure 2-8 : The strain condition of 3 beams under 10kN vertical loading and around 1.35MPa prestress, blue area indicate strain dur to compressive stress while red area indicate strain dur to tensile stress.

14

2.3.3 Numerical validation

2.3.3.1 Numerical model

Two types of numerical models(1D and 3D) for beam 1 under 4-point bending are established with DIANA FEA software. Considering the linear material assumption, the linear elastic isotropic material model is selected with a linear elastic analysis in the numerical model. Both of the models are using the same geometry, loading and supporting conditions, as well as material properties, presented in Appendix D.

To support the analysis of numerical results, the analytical calculations are presented through the function below to calculate the deflection at the mid-span due to 4-point bending. The value of the input is derived from the numerical models.

$$\delta = \frac{(F/2)a}{24EI}(3l^2 - 4a^2) = 0.0626mm$$

Young's modulus (E): 30000MPa; The vertical load (F): 10000N; The distance between loading point to adjacent support point (a): 400mm; The support span (l): 1200mm; the moment of inertia (I): 163234000mm4.

By comparing the numerical data with the analytical results, the 1d hollow model has the same deflection value as the analytical results. This is clear evidence of the 1d modelling is based on the basic Euler–Bernoulli beam theory. The 3d hollow model deflects more than 1d hollow models, which is possibly a result of the mesh sizes and element types. There are mesh sensitivity studies to elaborate on the influence of different mesh sizes and also the various mesh size impact on different elements. In general, a smaller mesh size will result in more accurate results for linear elements. [17] Due to the limitation of the educational version for DIANA FEA, 10mm is the minimum mesh size available for the 3D model. As the result, it is important to consider the deviation compared to the theoretical calculation during the following analysis. Based on the analysis above, the author decided to use 1d models for load-displacement comparison, while the 3d model for the comparison of strains due to prestressing and bending of beam 1.

2.3.3.2 Numerical result analysis

The 1d numerical model is established as the simulation of the 4-point bending test (maximum 10 kN) of beam 1. The material property and geometrical dimensions are derived from the digital design. There are 2 loadings applied in sequence, the prestressing force (divided by 10 steps) at first and then the vertical load until 10 kN(20 steps). The property and result comparison are shown in table 2-1.

	Young's modulus	Middle moment of inertia	Prestress force	Prestress distribution	Maximum vertical load	Displacement at peak load
1d model	30 GPa	163234000 mm4	30kN	Centric Evenly distribute	10kN	0.0626 mm
Experimental test	Unknown	Unknown	30kN	Eccentricity at minus z direction	10.015 kN	0.0269 mm

Table 2-1: the parameter comparison between 1d model and experimental test of beam 1.

It is obvious that the displacement at the peak load of the test is less than half of the value of the 1d model. Considering the material properties and test geometries, there are 3 possible influence factors resulting in this gap: Young's modulus variation, geometric deviation and the bending moment benefit from the eccentricity of prestress. Firstly, Young's modulus of the material is not clear, indicating the possibility of a higher number for actual material compares to the assumed value. To verify this

influence, a series of 1d models with Young's modulus as the only variate. The results show similarities to experimental performance when the Young's modulus reaches 70 GPa, which is far beyond the common Young's modulus value of the concrete. As the result, the influence of Young's modulus can only be part of the reason for the displacement gap between the model and test.

The geometry differences are another possible reason leading to higher stiffness in the experimental test. As the printed geometry can be influenced by a variety of parameters(pump pressure, material status, etc.), the dimension of the experimental beam can vary from the designed value. The accurate cross-section dimensions in the middle of the beam are hard to measure, especially for thickness measurement. Several 1D models with changing height and thickness have been established, to verify the influence of geometric values. Referring to the numerical results, a similar test deflection can be obtained with approximately 43% increase in the cross-section area. This geometry difference exceeds the tolerance of printing deviation, thus the geometry difference can only be regarded as partly influencing the deflection results.

The eccentricities of the prestress can also result in smaller deflection. There is an assumption from the numerical model that the prestress force is applied in the centre of the beam cross-section, indicating no extra bending moment results from prestressing force. It also assumes the uniform distribution of the prestress force. However, according to the strain data analysis in chapter 3.3.2, the existence of prestress force eccentricity has been proven. The eccentricity at the minus z direction of the prestress force will introduce a positive bending moment at the tension area, resulting in less bending moment at the mid-span, hence, the displacement at the mid-span will be reduced. The influence can be calculated based on the static beam equations as follows:

$$M = -EI\frac{d^2w}{dx^2}$$

M: bending moment; w: deflection; E: Young's modulus; I: area moment of inertia

Young's modulus	Moment of inertia	Eccentricity (mm)	0	10	20	30	40
30 GPa	163234000 mm4	Displacement at mid-span (mm)	0.0626	0.0516	0.0406	0.0296	0.0185

Table 2-2: the calculated results with different eccentricity distance.

Table 2-2 show the calculation results with various eccentricity distances, on the condition of the same material properties. The displacement at the mid-span will have a sharp decrease with little effort in adding eccentricities. Around 30 mm eccentricity in the minus z direction can result in a displacement value similar to experimental performance. It can be deducted that the difference between the numerical model and the experimental test is mostly influenced by the eccentricities of prestress force and only partly influenced by Young's modulus and geometry variation.

The 3D model in DIANA FEA has been prepared to generate the strains under ideal geometry and loading conditions, at the same location as actual strain gauges. Due to the computational effort and the limited element numbers, only half of the beam has been simulated, with loading and supporting conditions shown below. The basic material input is the same as the 1d model.
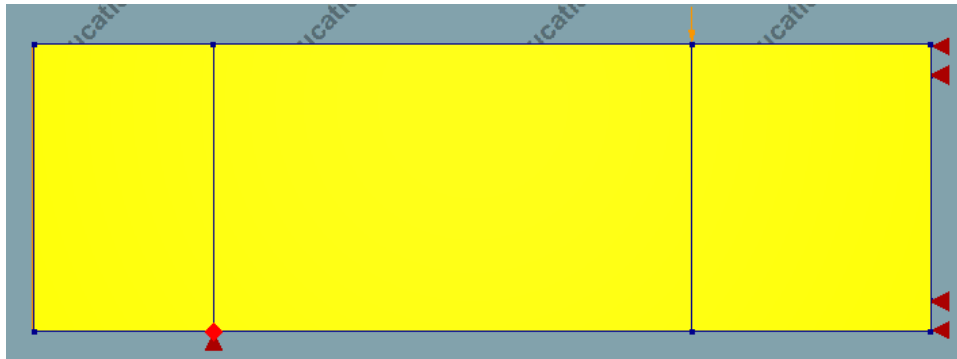
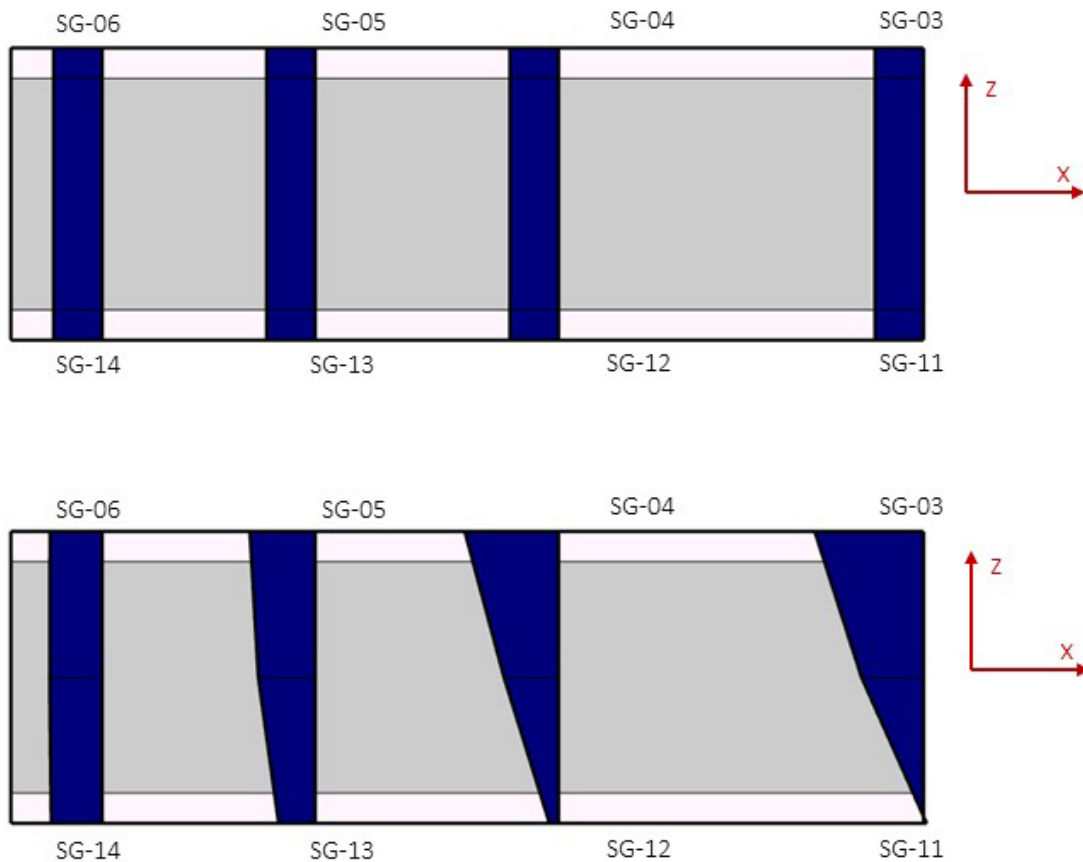*Figure 2-9: The loading and supporting conditions in 3D model*

Figure 2-10: The strain distribution of the side surface in x-directions under pure prestressing(top), vertical loading and prestressing(bottom) of 3D hollow cross-section model.

The strains at the bottom edge, middle side surface and the top edge (in the location of physical strain gauges) are collected. According to the results, these strain points show the same value due to prestressing, indicating an evenly prestress distribution in the model, which varies from the uneven distribution under pure prestressing in the test. The deformation is also collected at the same points while applying the vertical load. As shown in the figure 2-10, there is a nonlinear behaviour from the bottom to the top surface of the beam in the tension area. This regional nonlinear behaviour possibly results from the thin wall structure. To verify the suspect, a 3d model with a solid cross-section as only variation is established. The strain behaviour along the side surface performs linearly in this 3D solid model, under the same conditions. It proved the strain in the x direction is influenced by thin wall

_____

geometry. These numerical results also claim the importance of measuring the side surface deformation in the experimental test, to further investigate the material behaviour.
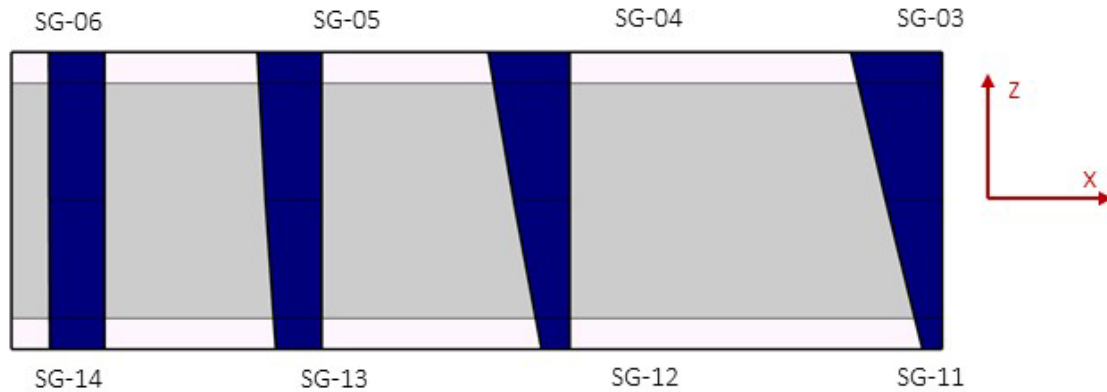
Figure 2-11: The strain distribution of the side surface in x-direction under bending and prestressing of 3D solid cross-section model.

2.4 Assessment of the structural design

According to the validations above, the whole structure shows linear-elastic behaviour under bending and prestressing based on load-displacement curvature. The 3D numerical results indicate the possibility of regional non-linear behaviour. But due to the invalid data collection from the DIC method, the proof of local material behaviour is not sufficient. The loading condition assumption for prestressing is verified as invalid, based on the experimental deformation under pure prestressing collected by strain gauges. The 1D numerical model explored the influence of prestressing eccentricities. Nonetheless, the prestress distribution is possible to be improved by introducing a bulkhead at the end of the structure, to confine prestress locations(avoid negative eccentricities) and benefit for even stress distribution. The 1D numerical model also suggests the influence to structure behaviour from Young's modulus variation and geometry differences. These variations should be taken into consideration for furthuer development of the structural design tool. For example, investigate the variation between printed elements and designed dimensions, and transform this variation as influence factors in the structural design tool. The experimental results of 3 beams, which are as expected, demonstrate the feasibility of using this structural design tool for material optimization.
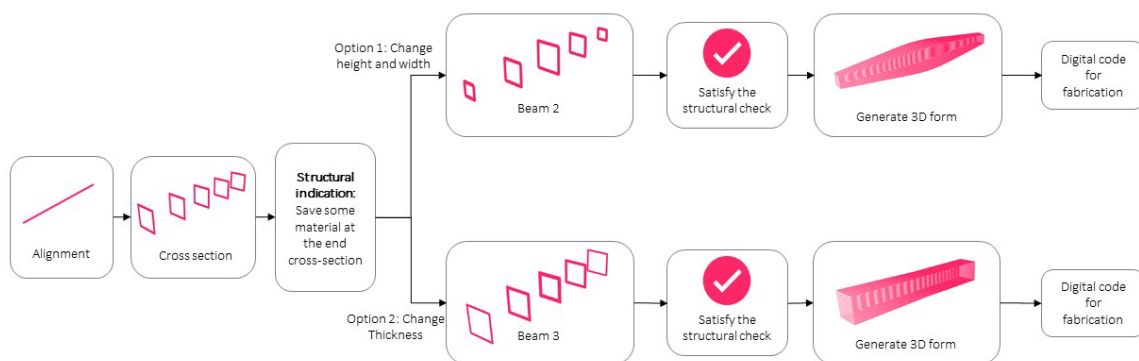

Figure 2-12: The simplified instruction of structural design tool.

Above all, this structural design tool is proved to be a reliable preliminary version for basic structural checks and material optimizations of 3DCP structures. A simplified instruction for using this tool is

presented in figure 2-12. Several developments can be implemented to this structural design tool as well. The improved experimental tests should be involved to investigate the tolerance between design and physical performance. More loading conditions should be considered in future development. The detailed recommendation will be discussed in chapter 5.

Chapter 3. Design of dry connection

This chapter aims to explore the practicability of the dry connection concept with 3DCP technology. At first, the design criteria for dry connections will be introduced separately as interlocking shapes and interlayer material. Followed by a detailed explanation of the design approach and procedure for each topic. A validation is obtained to verify the design of dry connections and the assessment of this design will be elaborated at the end.

3.1 Design criteria

The "dry" connection concept is generated and involved in this project, including the design of an interlocking shape(utilizing the form-freedom of combined robotic additive and subtractive manufacturing) and a soft interlayer material between elements. Considering the material properties, loading and supporting conditions, as well as the fabrication process of the 3DCP structure, the criteria for dry connections can be listed:

- **Mechanical properties**

Compare to the monolithic structures, the structures with dry connection have less structural integrity, especially behave weaker at the connection area. It is important to have a shear capacity requirement at the connection so that the structure can work as good as monolithic elements. The interlocking shape should also avoid stress concentration which can easily lead to flaws and brittle fractures. Because the dry connection structure is assembled with the prestressing system, the soft interlayer material should be able to withstand long-term compressive stress. The deformability of the interlayer material is also very important as it should be soft enough to fit the interlocking shape, while not too soft so that the deformation in the other directions is limited.

- **Manufacturing requirements**

The 3DCP technology helps to realize the interlocking shapes but also restricts the designed shape, such as the limited amplitude value. In this project, the limitations will be considered according to the fabrication with the 3DCP facilities at TU/e. Besides, there are deviations between the design and printed elements, which will worsen the connection tolerance in reality. This situation can be improved by the milling process to result in a more precise contact surface.

- **Sustainability and durability**

The final products will be used in bridge structures, which usually have more than 50 years of service life. As the result, to decrease the maintenance requriements, the interlayer material should be durable in an outdoor environments (resist water, freeze-thaw cycles, UV light etc). The interlayer material should also be sustainable enough to reduce the carbon footprint.

3.2 Prototyping procedure
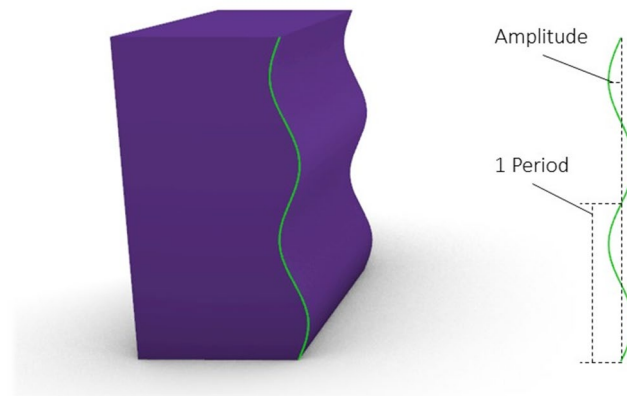
3.2.1 Method of interlocking shape design

Figure 3-1: The schematic of sine interlocking shapes, amplitude is the maximum change of the wave in the direction perpendicular to wave propagation direction; 1 period involves the wave to complete one cycle.

Since the concrete is brittle, the conventional tenon joint or key joint will concentrate the shear force in a relatively smaller contact area. It can result in the break of the connection, thereby the failure of the whole structure. Hence, the author decided to adopt a sine shape which is presented as gentle convex for interlocking design. The sine waves will bring a smooth change of the contact surface so that the sharp angles will be avoided, as the schematic shown in figure 3-1. The exact frequency and

_____

amplitude of the sine shape will be designed based on numerical suggestions and manufacturing allowance.

To better understand the structural behaviour of different sine shapes, a set of numerical models is formulated in DIANA FEA. The model simulates half of the triplet shear test for solid concrete bricks. The classical Mohr-Coulomb friction property is applied to the interface between two bricks. A prescribed 2mm displacement in the minus y direction is given to the middle brick in the model. Aiming to investigate the shear capacity of different interlocking shapes, the reaction forces and concentrated stresses will be compared and discussed. The numerical models are established based on several assumptions:
-   Linear material behaviour
-   Solid structures with even distributed force and load
-   Assumed friction coefficient and zero cohesion at the contact surface
These assumptions indicate the possibilities of different behaviour in the physical world, thus, experimental validation is required.

The first set of numerical models is focused on the influence from the increasing period of sine shape, as shown in figure 3-2. According to the relevant reaction forces(in Appendix E), which have a significant increase with the growing frequency(more period involved) of the sin shape. It indicates the interlocking shape with more periods of sine wave will perform better to resist the shear load. The stress condition at peak load is presented in the same colour scale as the figure below, which shows increased concentrated stress(dark blue area) with the growing frequency of the sine shape. This concentrated stress is not favourable in interlocking shapes. Thus, further investigation is required to generate optimal solutions which have not only good shear capacity but also affordable concentrated stress.

(a)   (b)   (c)   (d)
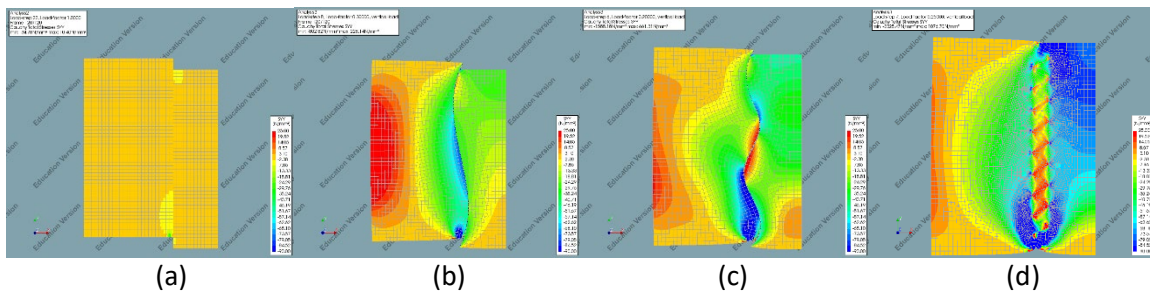
Figure 3-2: The stress distribution in y direction of interlocking model with straight connection(a); sin shape with 1 period, 4mm amplitude(b), sin shape with 2 period, 4 mm amplitude(c); sin shape with 10 period; 4mm amplitude(d).

The second group of numerical models aims to investigate the influence from different amplitudes. A set of models with the same period but different amplitudes are established, with the same loading and supporting conditions as above. According to reaction forces, the results show a positive effect from amplitude increase, indicating that the sine interlocking with higher amplitude performs better under shear load. As shown in figure 3-3, the stress distribution for each model is presented in the same colour scale. It is obvious that the stress concentration increased due to the growth of amplitude. Therefore, it is also necessary to consider the balance between good shear capacity and less stress concentration in defining amplitude values.
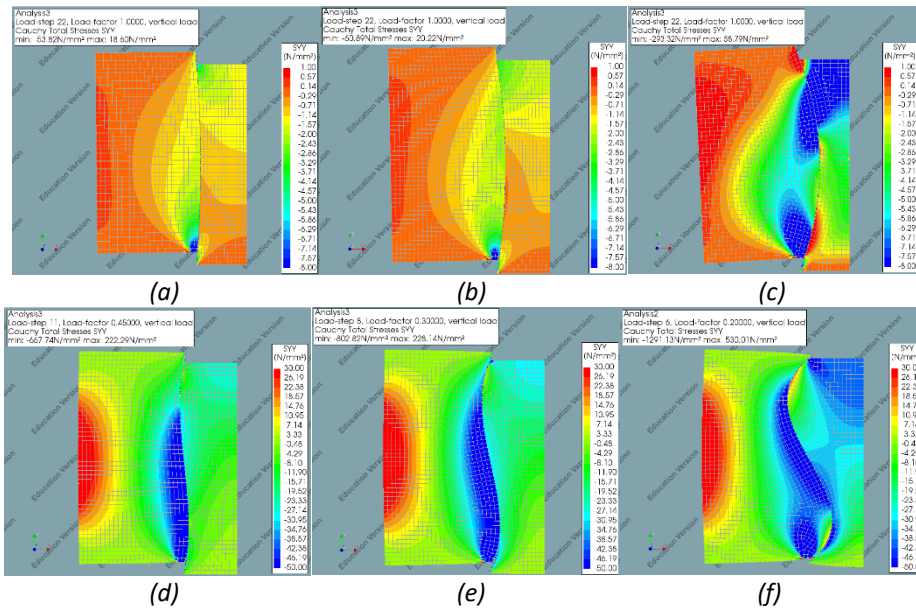
_____

Figure 3-3: The stress distribution in y direction of interlocking model with sine shape at 0.5 period, 2mm amplitude(a); sine shape with 0.5 period, 4mm amplitude(b), sine shape with 0.5 period, 10 mm amplitude(c); sine shape with 1 period; 2mm amplitude(d); sine shape with 1 period; 4mm amplitude(e); sine shape with 1 period; 10mm amplitude(f)

Besides investigating the shear capacity of interlocking shapes, the research of manufacturing limitations should also be taken into consideration. Before applying the hybrid process to fabricating dry connected segments, the optimal milling process should be prepared.

Figure 3-4: The printing process(left) and milling process(right) of printed bricks.

The milling process will be implemented on the fresh state concrete surface as the milling of hardened concrete costs too much energy and creates a large amount of dust. Revealed from the research from Loughborough University, a spindle motor is selected to smooth the 3d printed concrete surface. [18] Taking account of the available robots and the safety issue in the TU/e concrete lab, a lightweight spindle motor is employed with the 6mm diameter, square shank edge drill at the end. A group of milling tests is proceeded to 3D printed concrete bricks, through shank milling (robot movement speed at 25mm/s) at different Revolutions Per Minute(RPM) at various concrete states. The test results (presented in Appendix F) suggest a higher RPM and a lower robot speed to mill at around 1.5hr after concrete printing. It is worth mentioning that the concrete state is also affected by environmental

_____

temperature and humidity. Thus, for a more precise conclusion, the printing and milling session should be implemented with environmental control.

On basis of the printing and milling system, several attempts are implemented to print different interlocking shapes. According to these test results, the prototype of interlocking shapes is designed as 1) sine shape with half period and 4mm amplitude; and 2) sine shape with full period and 4mm amplitude. The experimental tests will be implemented to verify the positive effect from designed interlocking shapes.

3.2.2 Method of interlayer materials design

Even though the milling process is been introduced to improve the connection area, there are unavoidable small protrusions at the contact surface, which can lead to stress concentration. This local concentrated stress will eventually produce cracks and propagate until failure. It is highly recommended to apply the soft interlayer material between the connections such that the stress can be redistributed evenly.

According to the compression test for osteomorphic blocks [19] and the triplet masonry test [20], polyurethane(PU) rubber and cork can be suitable candidates for interlayer material. The PU rubber 90 shore A with 3mm thickness is selected for this project, due to its high resistance to compressive strength and good performance in exterior space. The 3mm thickness also allows it to deform into interlocking shapes. For sustainable perspective, the 4mm cork board from Amorim is therefore been prepared. The cork board has a zero Poisson's ratio so that it will deform but not expand in the other directions under any compressive strength. A series of triplet shear tests will be implemented for the combinations of different interlocking shapes with both interlayer materials in the following chapter. The result will verify the influences from the selected interlayer material.

Advantage	- Excellent deformability - No deformation in lateral direction - Easy to prepare - Completely recyclable	- Great anti-pressure ability - Good deformability - Great performance in outdoor enviornment
Disadvantage	- The anti-pressure ability is not excellent - No predictive behaviour before failure - Less resistant in outdoor environment	- More difficult to recycle - The deform in lateral direction limited the allowed compressive stress

Figure 3-5: The selected cork board interlayer(left) and PU rubber interlayer(right).

24

_____

3.3 Validation of the dry connection prototypes

3.3.1 Validation ambitions

As mentioned beforehand, the interlocking shape is designed upon several assumptions, it is necessary to validate the dry connection design for 3DCP structures. Also, there are 2 selected interlayer materials, each with its own unique advantages. It is worthwhile to embed the interlayer material with interlocking shapes in the experimental test. Considering the basic design criteria and available lab facilities, the triplet shear test is introduced. Within these tests, not only the shear capacity can be tested, but also the ability of interlayer material to bear prestress can be verified.

3.3.2 Experimental set-up

Because of the limitations of the lab facilities, the dimension of test samples is restricted to 10cm*10cm*5cm bricks. This size is also convenient for manufacturing and material saving. Since the test is a set of 3 bricks, the middle brick required a double curved surface. Thus the manufacturing process starts with the printing and milling of a basement, and then the bricks can be printed on the shaped basement to generate double curvatures. 3 types of interlocking shapes are prepared, known as the straight connection(no interlocking), the sine shape with half period and 4mm amplitude, and the sine shape with full period and 4mm amplitude. There are 3 types of interlayer material options, defined as no interlayer(concrete to concrete), cork board interlayer and PU rubber interlayer. Each type of interlocking shape will group with each category of interlayer materials. There are three groups of bricks for each combination to obtain more accurate results through average values. The test set-up is shown in figure 3-6. The three bricks are assembled with horizontal prestressing force(0.5MPa), the two supports are under two side bricks while the vertical load is applied to the middle brick. The applied force and corresponding displacement will be recorded automatically until the middle brick is pulled out or until failure.

| (a) | (b) | (c) |
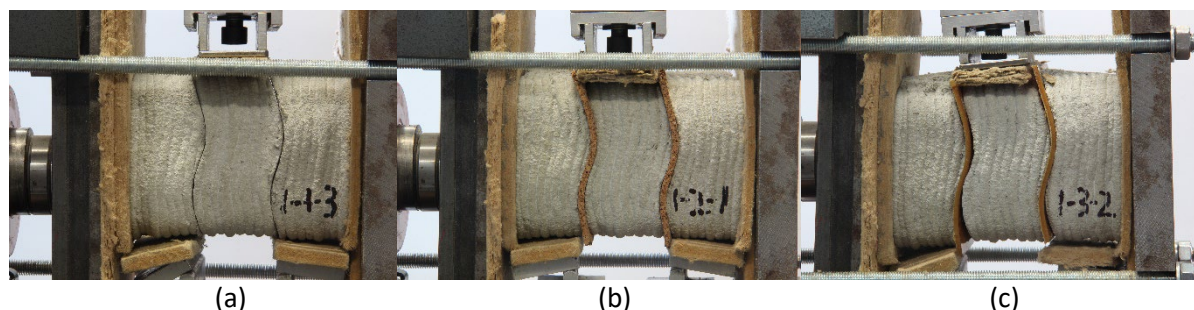
Figure 3-6: The triplet shear test for full sin shape with no interlayer(a), cork interlayer(b) and PU rubber interlayer(c).

3.3.3 Experimental result analysis

Based on the experimental results, most middle bricks in the straight connection or half sine shape connection is slid out at the end of the test. While for the full sine interlocking shape, the test is mainly finished with the appearance of a crack. The sliding distance for the full sine interlocking shape is less obvious compared to the other shapes. It is consistent with the numerical analysis in the design process, that the interlocking with a higher period in the sine wave will fail due to the concentrated stress. In addition to the interlocking shapes, both interlayer material has no obvious lateral deformation due to prestressing, through observation. Part of the test results are exhibited in Appendix G. Since no failure or crack happened to most of the straight connection and half sine interlocking shapes, the reaction

force at the first slide is selected for analysis and comparison. The result is presented as the sliding load for different groups in chart 3-1.
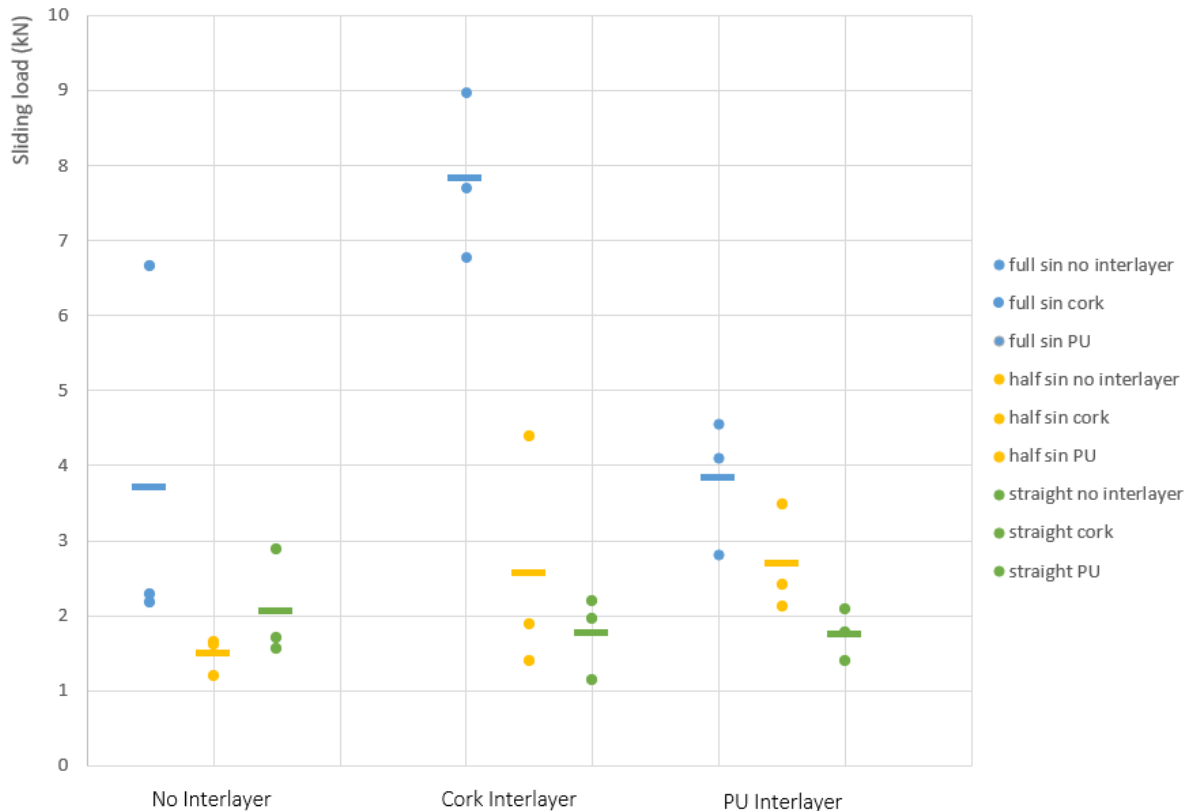

Chart 3-1: The experimental result of sliding load for different dry connections, the short line represent for average value for each type.

Comparing the sliding load on all straight connection groups, the interlayer material has little influence. The average sliding load even has a slight drop when adding interlayer materials, which can result from a smaller friction value between the contact surface. However, the advantage of interlayer material appears when the interlocking shapes are introduced. As shown in the chart above, both interlayer has positive effects on curved interlocking shapes, especially the cork board which has a more remarkable benefit. When comparing the sliding load between different interlocking shapes, it is more obvious to find the superior, with the evidence of all blue points(full sine shape) has a higher sliding load. The half sin interlocking shape also performs better than straight connections.

This triplet shear test result proves both of the designed interlocking shapes have a positive influence on their shear capacities. While the selected interlayer material is suggested to work with interlocking shapes to show their advantage. Some test values have relatively large differences compared to other groups, thus these test results can only provide the first indication but more extensive experiments will be required for future investigation. Overall, the cork board interlayer with a sine shape(1 period and 4mm amplitude) is regarded as the best solution for dry connections.

3.4 Assessment of the dry connection design

Through the validation, the design options for interlocking shapes and interlayer materials are proved and verified. The interlocking sine shape connection is verified to be able to increase the shear capacity at the contact area compared to straight connections. Meanwhile, the selected interlayer material also helps the connection to resist shear force. The failure mode of the experimental test presents conformance with the numerical analysis during the design process, which indicates the correctness

of the design approach. However, this design is only considering small-scale digital manufacturing and low prestressing level. To extend this dry connection design to industrial applications, the tests at different scales should be investigated. In general, the design of a dry connection is applicable for circular designs of 3DCP bridge elements. The user can involve the dry connection design in the 'segment' phase of the design tool, with a detailed explanation in Matthew Ferguson's EngD report.

Chapter 4. Structural design applications

In this chapter, the application of structural design tool and dry connections will demonstrated with different user stories. Through the explanation of these user stories, the practicality of the structural design and dry connections can be addressed in various senarios.

_____
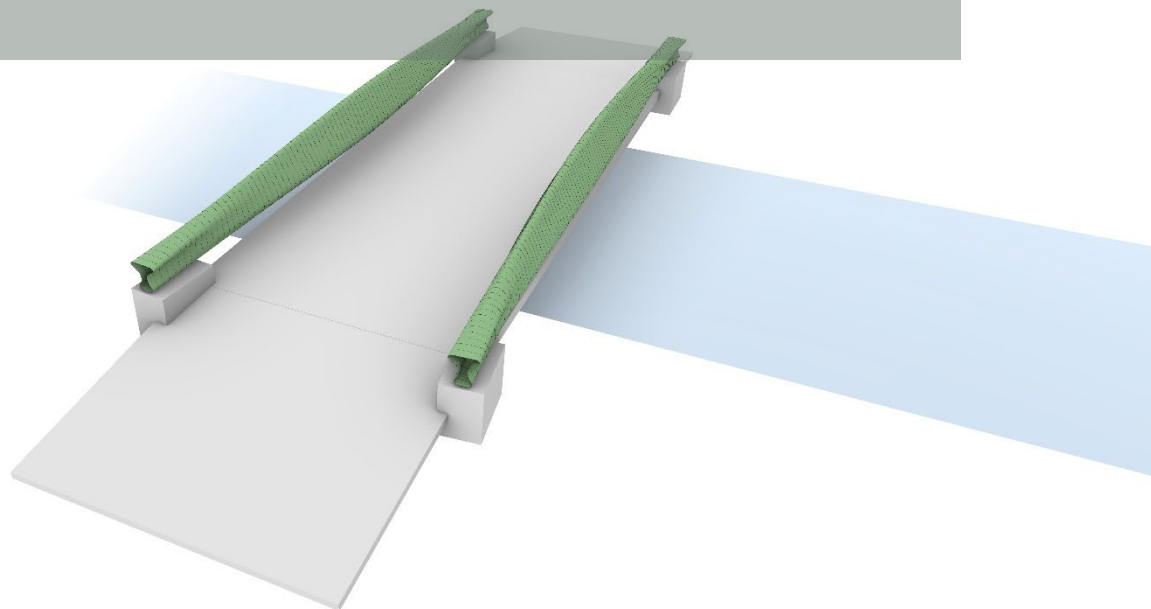
4.1 The application of structural design tool

User story 1: free-form bridge
"As an architect, I want to design a peculiar pedestrian bridge with less material use, so that I want to know if my design is buildable or not at the earlier stage."

To generate a free-form structure, the structural design tool can guilde the user to shape their design from material optimization perspective, through changing the input such as height, width of cross section, thickness of cross section, support locations and prestressing eccentricities. A detailed workflow with possible solutions are shown below:

_____
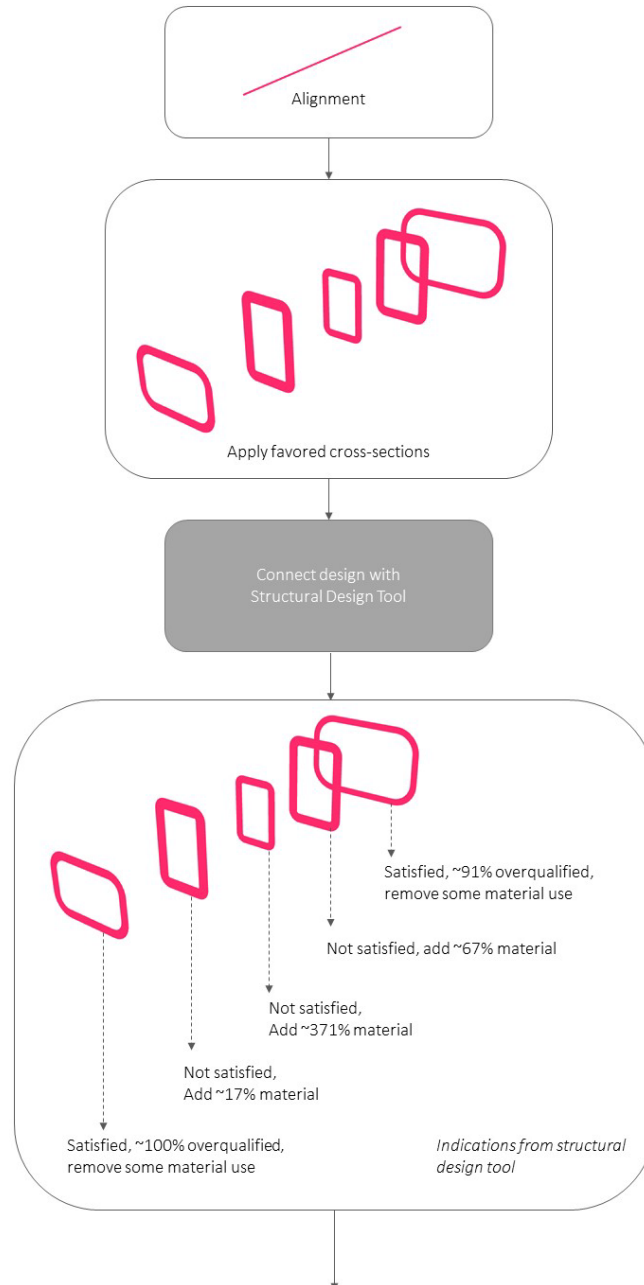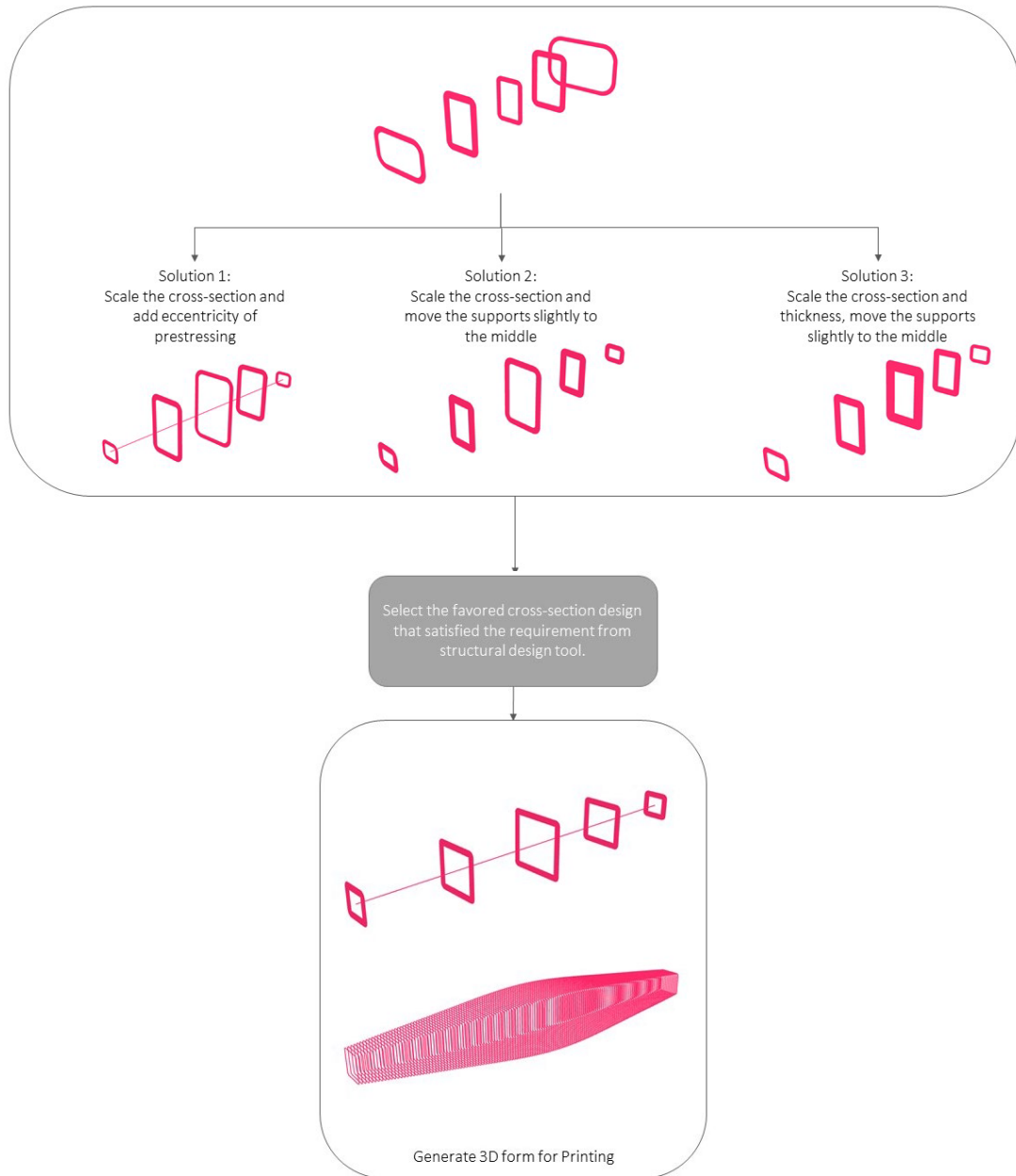
Figure 4-1: The workflow of using structural design tool.

User story 2: Bridge with boundary limitations
The project aims at design a feasible bridge on a river where has waterway transporation. The requirements is the support points are fixed and the height of the structure should not exceed 200mm.

According to the requirement of this project, the design freedom is limited. With the help of structural design tool, the user can still adjust their design in thicknesss, width of cross-section or add eccentricity of prestressing to generate a buildable structure.

Step 1:
Draw favored alignment between 2 support points across the river.

Step 2:
Connect cross section geometry with structural design tool.

Step 3:

Adjust the width of cross-section, change the thickness, add eccentricity of prestressing to help the dimension satisfy the structural requirement.

Step 4:

Define cross-section and prestress locations. Gnerate 3D form and relevant informations for digital manufacturing.

4.2 The application of dry connections

User story 3: reusable bridge

The project aims at design a bridge with 50 years service life, with a possibility to be rebuild after its service life to fit increasing traffic load.

Considering the reusability of structures, the dry connection design can be implied to the design process. The designed shape can be shaped and manufactured as segments, which will assembled with prestressing system and interlayer material in between. After its service life, the prestress can be released, and structure can be disassembles and rebuild with the requirement of new structures.

This dry connection design can also be used for temporary structures due to its easy assembly and disassembly process.

3D form   Insert interlocking shapes   Generate segments with dry connections
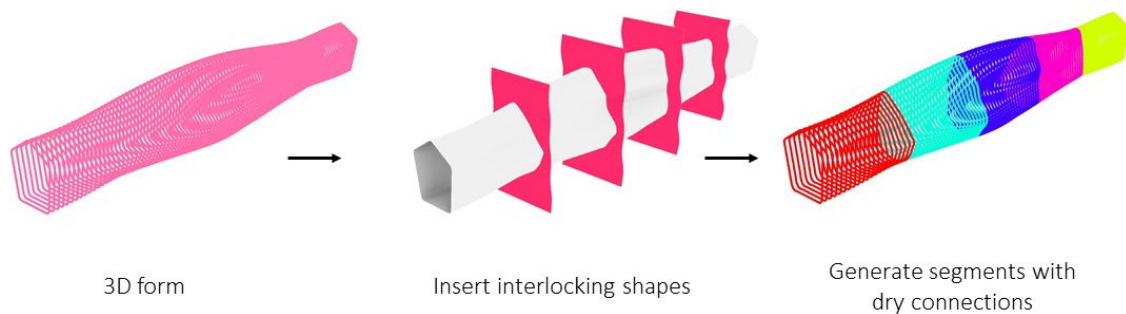
Figure 4-2: The dry connection design through design tool.

Chapter 5. Disseminations

In this chapter, several dissemination activities relates to the project will be introduced. The project influence, feedback and lessons learned from each activity will be discussed.

_____

BE-AM
BE-AM is a symposium and exhibition for 3D printing and the addictive manufacturing held annually. A beam designed from the digital workflow was exhibited in the BE-AM 2021. The beam is designed with the helpf of the structural design tool. It was printed in segments and assembled with a steel bar under prestressing. Since the dry connection concept was not well investigated at that time, the beam is assembled with timber elements as interlayer material to present the dry connection idea.

The exhibited beam attracts public attention to the digital workflow of the 3DCP structure, and it shows the possibility of demountable connection ideas. The difficulties in the assembly process enhance the importance of the interlocking shape design and the determination of prestressing locations.

Figure 5-1: The beam designed and manufactured through digital workflow exhibited in BE-AM event.

Digital Concrete 2022
The Digital Concrete 2022 is a conference for exhibitions, communications and discussions on concrete and digital fabrication. It involves developments and innovations in both academia and industry. This project was presented as a poster at the conference, as shown in Appendix H. Through the discussion with researchers and engineers, the digital workflow and dry connection concept is been discussed and supported by many participants.

Through this Digital Concrete conference, the development of printable material brings chanllenges and possibilities to the digital workflow and dry connection. The innovative testing and fabricating method introduces the chance to improve the validation process.

_____
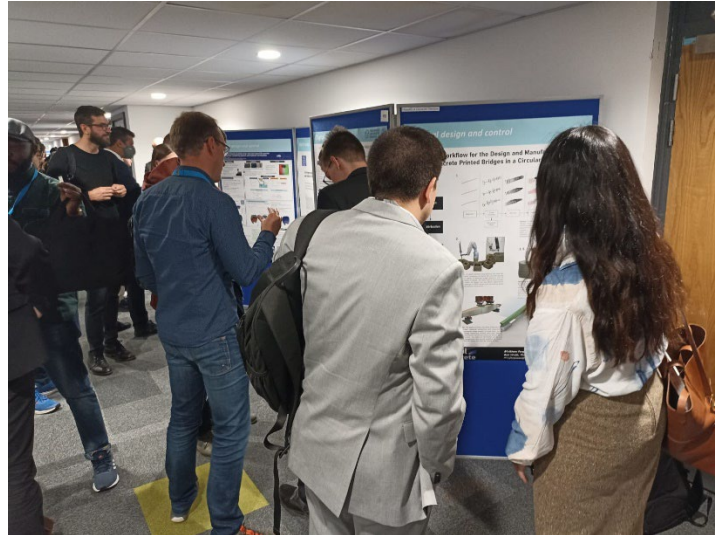
Figure 5-2: The poster session in Digital Concrete 2022

Dutch Design Week

Dutch Design Week is an annual design event for design projects or concepts in different fields.

Figure 5-3: The Dutch Design Week event in Ketelhuisplein, 2021(left), The final prototype for Dutch Design Week 2022, printed in Vertico(right).

A 2-meter beam designed with the digital workflow will be presented in the Building The Future sector of Driver of Change exhibition. It will be printed in segments with interlocking shapes to show the dry connection concept. A poster will be presented beside to show the rendering of designed bridge structures. A short video will be shown as the explanation of the development process of this project. It will be a great platform to highlight this project to a wide audience and the press. The preparation process to attend this event helps the author to sum up the progress and results of this project.

Chapter 6. Conclusions

In this project, the structural design tool embedded in digital workflow and the dry connection prototype is designed and validated, with consideration of improving productivity and sustainability. At the end of this project, the conclusion will be addressed for each deliverable, along with suggestions for future development.

_____

6.1 Conclusion

Structural design tool
A structural design tool has been developed in the same working environment as the digital workflow. This structural design tool can provide users with the real-time structural feedbacks and indications of prestressing location. The material optimization with ensured form freedom can be simply realized with this tool.

This structural design tool is generated based on several assumptions. The validations are obtained to verify the assumptions of linear material, structural input and loading scenario. The experimental validations are implemented to 3 beams that are designed from the digital workflow. The result shows the linear structure behaviour under 10 kN vertical load and 1.35MPa prestress. The strain data collected from stain gauges proves an uneven prestress distribution along the beam axis, as well as the prestress eccentricity in the minus z direction. The comparison between experimental results and 1D numerical results presents the influence from Young's modulus, prestress eccentricity and geometry difference on structure stiffness. The 3D numerical results suggest the possibilities of thin-wall structure influences, which can be further investigated. As above, this structural design tool can be regarded as a preliminary version embedded in the digital workflow. Future developments are required to improve this structural design tool.

Dry connection
The design of dry connections has been explored in this project, focusing on the design of interlocking shapes and interlayer materials. The design of interlocking shapes aims at selecting sine waves with optimal amplitude and period value following the design criterias. The interlayer materials are selected as the cork board and PU rubber considering their mechanical properties, sustainabilities and durabilities.

The designed prototype has been validated through the experimental test. The triplet brick shear tests suggest that interlocking with a full period of sin wave has the best shear-resisting performance, compared to other interlocking shapes. The corkboard behaves better than PU rubber material at low prestressing conditions. Supported by validation results, this dry connection design can provide users with the possibility to design a reusable structure through this digital workflow.

Knowledge dissemination
The knowledge and information about this digital workflow have been well disseminated, through academic discussions, tests and evaluations in the lab, and through presenting physical products in public. By attending conferences and design events, the digital workflow concept and dry connection idea have been widely spread.

6.2 Recommendations and future expectation

This digital workflow is expected not only to focus on bridge(beam) structures but also to cover other structures, such as columns in building structures or slabs in road constructions. The growth of this digital workflow will be supported and influenced by the development of 3DCP technology and relevant material research. The detailed recommendations will be discussed below:

Development of structural design tool
- Involving unsymmetrical cross-sections or even in-fills.
  This structural design tool is based on basic beam theory with the assumption of the symmetrical cross-section. To simplify the calculation, only hollow cross-sections are

considered in this project. Therefore, to increase the design freedom, the calculation of unsymmetrical cross-sections with infill patterns should be involved in future development.

- Involving different loading and supporting scenarios.
  The structural design tool only considers the simply supported beam with the distributed load. The solutions for complex scenarios can be involved to provide users with more options. For example, the cantilever structure or concentrated load scenario.
- Introducing the Structural Health Monitoring System(SHM)
  The SHM system can be involved in the bridge structure during the in-service period. The structural performance can be collected by this system, which can be used as feedback to better understand the behaviour of 3DCP structures.

Improvement of validation

- Apply the DIC method to the 3DCP structure test
  As mentioned in chapter 2, the DIC method was applied during the experimental tests to verify the material behaviours on the side surface but failed due to the limitation of the measuring equipment. The DIC measurement is a very helpful method to capture strains without adding material to the observational objects. The strain measurement in the side surface is also very important for investigating the material behaviour of the 3DCP structure. Thus, it is worth developing the research relates to applying the DIC method to 3D printed structures.
- Investigate geometry differences
  In the numerical analysis, the influences from geometry differences are discussed briefly. A more detailed experimental validation can be involved. For example, introducing scanning technology to scan printed products so that they can be compared with designed models.

Improvement of dry connection design

- Compare dry connections with monolithic structures
  It is worth testing the shear capacity of monolithic structures so that the different performances compared to the same scale dry connections can be investigated. It helps the designer to make choices between sustainable dry connections or integral structures.
- Test the interlocking shape with different scales
  This project only designed and validated the dry connection in relatively small-scale structures. It is still not clear how the dry connection behaves on a larger scale. It is worth applying the relevant tests to investigate the dry connection performance in larger structures.
- Interlayer material behaviour under different prestressing levels.
  As described in chapter 3, the interlayer materials are only validated under 0.5MPa prestress, which is relatively low. To further research the interlayer material performance, different levels of prestressing should be applied while using these interlayer materials in different interlocking shapes.
- Durability of the dry connection
  Considering the in-service situation, the bridge structure is possibly under cyclic load. Therefore it is very valuable to involve the research of dry connection durabilities under cyclic load, which involves the interlocking performance and fatigue behaviour of the interlayer material. This research helps to establish the practicability of dry connection.
- Improvement of the milling process.
  While producing interlocking shapes, the hybrid manufacturing process was introduced. A simple selection for milling parameters was implemented with the observation of milled surface conditions in this project. For a more scientific result, the scanning technology can be used under controlled environmental conditions, to compare the states of milled surfaces, such that more reliable milling solutions can be generated.

Chapter 7. Appendix

Appendix A. Python code for structural check

```python
"""Provides a scripting component.
    Inputs:
        x: The x script variable
        y: The y script variable
    Output:
        a: The a output variable"""

__author__ = "rong"
__version__ = "2021.09.22"

import rhinoscriptsyntax as rs
import scriptcontext as sc
import ghpythonremote
sp = sc.sticky['sympy']
Function = sp.Function
Eq = sp.Eq
diff = sp.diff
dsolve = sp.dsolve
np = sc.sticky['numpy']
polyfit = np.polyfit
poly1d =np.poly1d


l0 = (L-l)/2
x = sp.symbols('x')
Mq = sp.symbols(b'Mq', cls=Function)
Vq = sp.symbols(b'Vq', cls=Function)
diffeqbmq = Eq(Mq(x).diff(x,x), -q)
BMq = dsolve(diffeqbmq, Mq(x), ics = {Mq(l0):0, Mq(l+l0):0})
SFq = Eq(Vq(x),BMq.rhs.diff(x))

f1= np.polyfit(xg,yg,2)
g =np.poly1d(f1)
Mg = sp.symbols(b'Mg', cls=Function)
Vg = sp.symbols(b'Vg', cls=Function)
diffeqbmg = Eq(Mg(x).diff(x,x), -g(x))
BMg = dsolve(diffeqbmg, Mg(x), ics = {Mg(l0):0, Mg(l+l0):0})
SFg = Eq(Vg(x),BMg.rhs.diff(x))


Mp = P*e

i = 0
while i < n:
    x0 = xl[i]
    A0 = A[i]
    I0 = I[i]
    w0 = w[i]
    S0 = S[i]
    b0 = b[i]
    Mq = BMq.rhs.subs(x,x0)
    Mg = BMg.rhs.subs(x,x0)
    Fq = SFq.rhs.subs(x,x0)
    Fg = SFg.rhs.subs(x,x0)
    fp = P/A0
    bendingstress = (Mg/w0)+(Mq/w0)-fp-(Mp/w0)
    compressionstress = (Mg/w0)-fp-(Mp/w0)
    shearstress = ((Fq+Fg)*S0)/(I0*b0)
    if bendingstress < ftk and shearstress < ftk and compressionstress > fck:
        indicator11 = (bendingstress-ftk)/ftk
        indicator22 = (shearstress-ftk)/ftk
        indicator33 = (compressionstress-fck)/fck
```

```python
        print ("satisfied", "{:.0%}".format(indicator11), "{:.0%}".format(indicator22),
"{:.0%}".format(indicator33))
    else:
        indicator1 = (ftk-bendingstress)/ftk
        indicator2 = (ftk-shearstress)/ftk
        indicator3 = (fck-compressionstress)/fck

print("{:.0%}".format(indicator1),"{:.0%}".format(indicator2),"{:.0%}".format(indicator3))
    i = i+1
```

Appendix B. Experimental test for 3 glued beams.
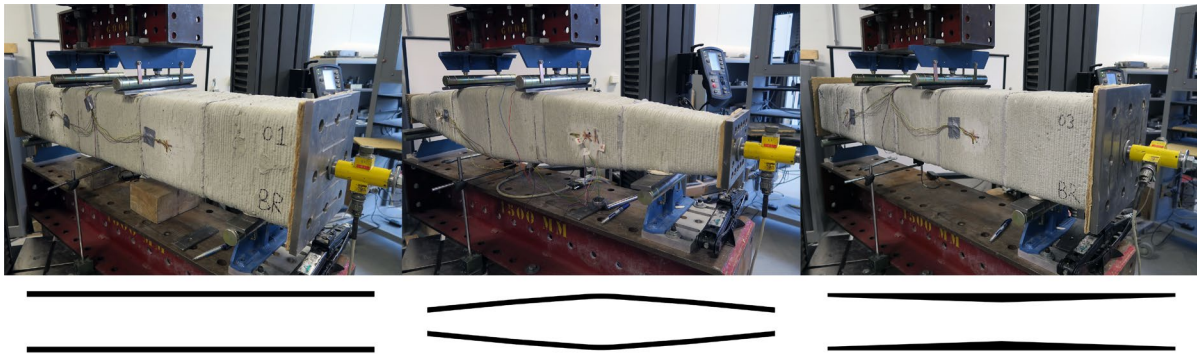
Figure 7-1. Four-point bending test for glued beam I, beam II and beam III (left to right), with corresponding representative geometry below

		Unit	Beam 1	Beam 2	Beam 3
Result from reference material samples	Average compressive strength	MPa	63.01	53.57	61.05
	Average flexural strength	MPa	5.85	5.60	6.14
Results from 4-point bending test	Horizontal prestress	MPa	2.7	2.7	2.7
	Failure load	kN	28.61	25.39	34.57
	Weighted structural performance	kN/m3	953.5	1094	968.3

Table 7-1: The experimental results for glued beams.

_____

Appendix C. Experimental test for 3 beams.

	Weight	Height of end cross section	Width of end cross section	Thickness of end cross section	Height of middle cross section	Width of middle cross section	Thickness of middle cross section	Length
	kg	mm	mm	mm	mm	mm	mm	mm
Beam 1	60.4	240	240	24	240	240	24	1500
Beam 2	44.4	120	120	24	240	240	24	1500
Beam 3	54.5	240	240	16	240	240	33	1500

Table 7-2: The weight of printed beam and geometrical information generated from the design tool.
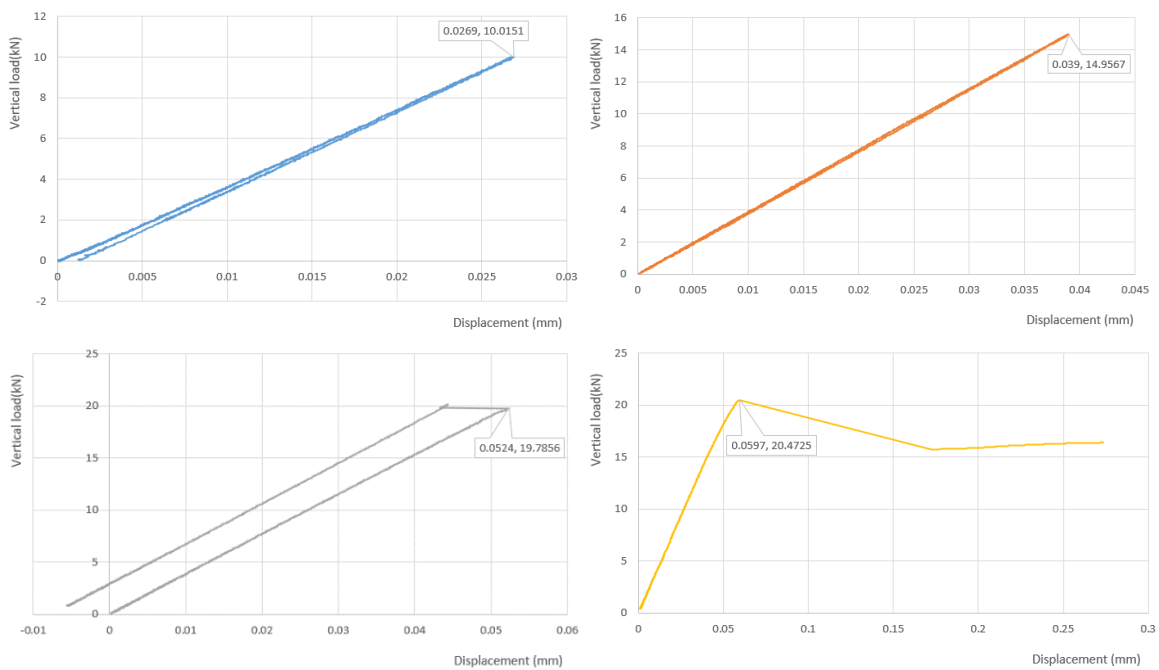
Chart 7-1 : The experimental load-displacement curve of beam 1.

43
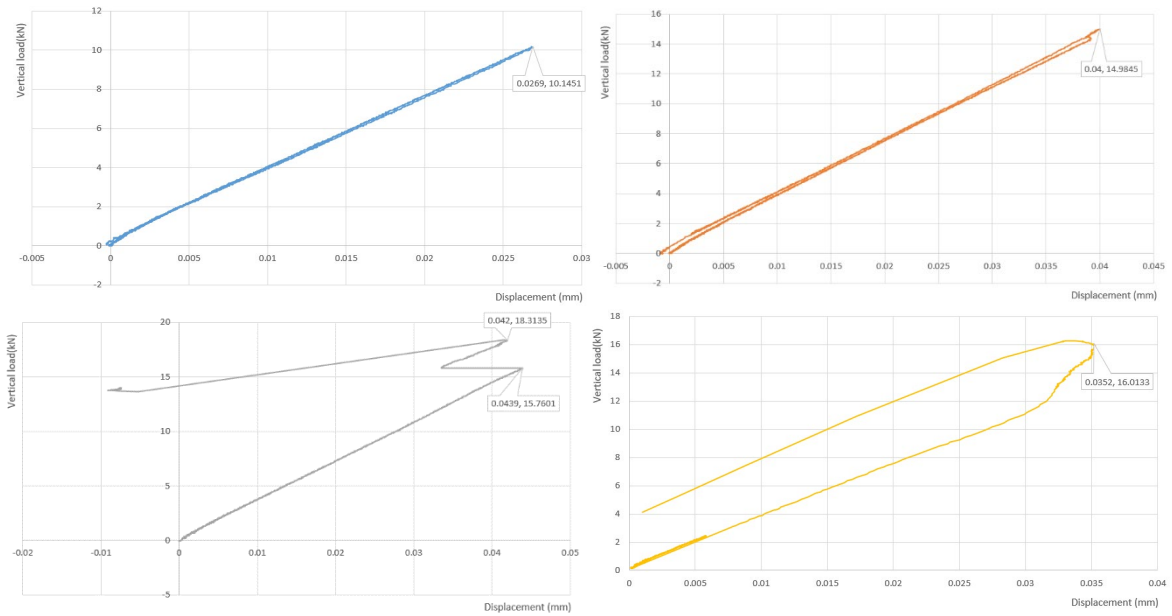
Chart 7-2: The experimental load-displacement curve of beam 2.
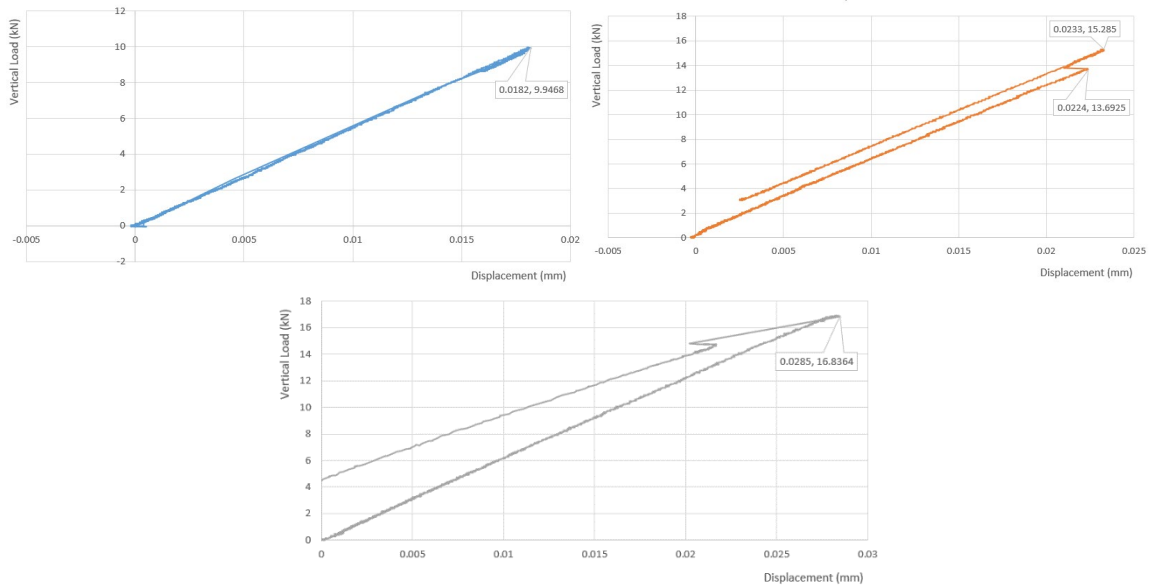
Chart 7-3: The experimental load-displacement curve of beam 3.

Appendix D. Numerical analysis.

		Model 1	Model 2	Model 3
Model properties	Dimensions	1d	3d	3d
	Mesh order	Linear	Linear	Linear
	Element type	L6BEN	CHX60, CPY39, CTE30, CTP45	CHX60
	Mesh size	10mm	10mm	10mm
	Cross section	Hollow	Hollow	Solid
Material properties	Material model	Linear elastic isotropic		
	Young's modulus	30000		
	Poission's ratio	0.2		

Table 7-3 : The basic information of the numerical models.
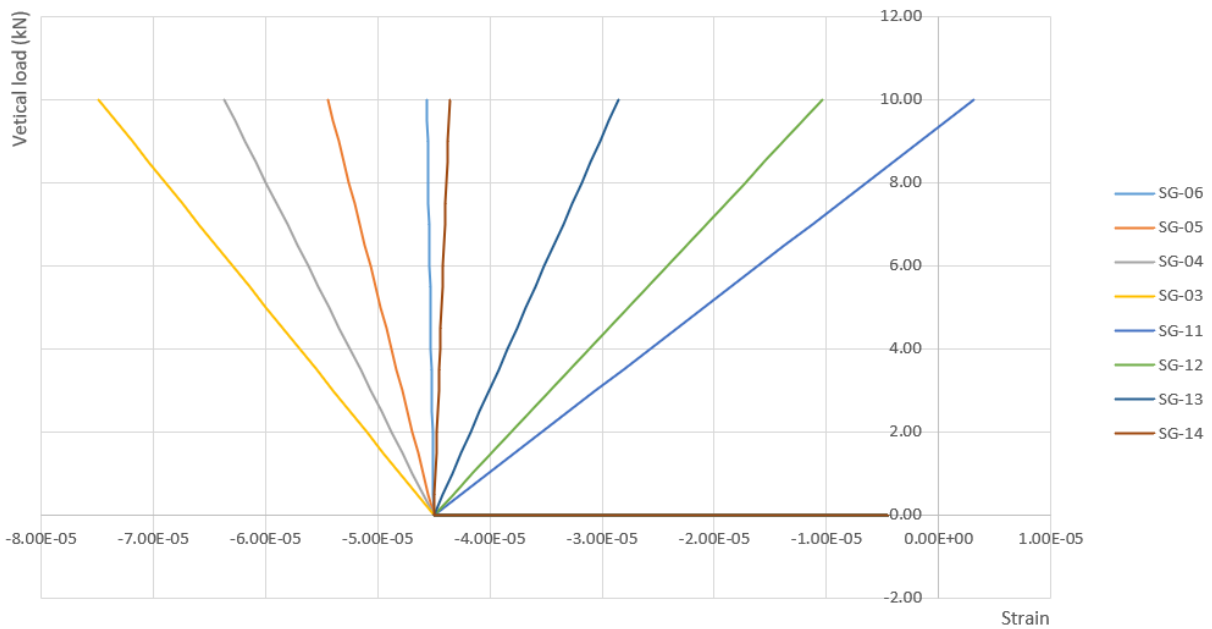
Chart 7-4: The strain distribution at strain gauge locations of 3D model of beam 1.

Appendix E. Numerical results for interlocking shape design.
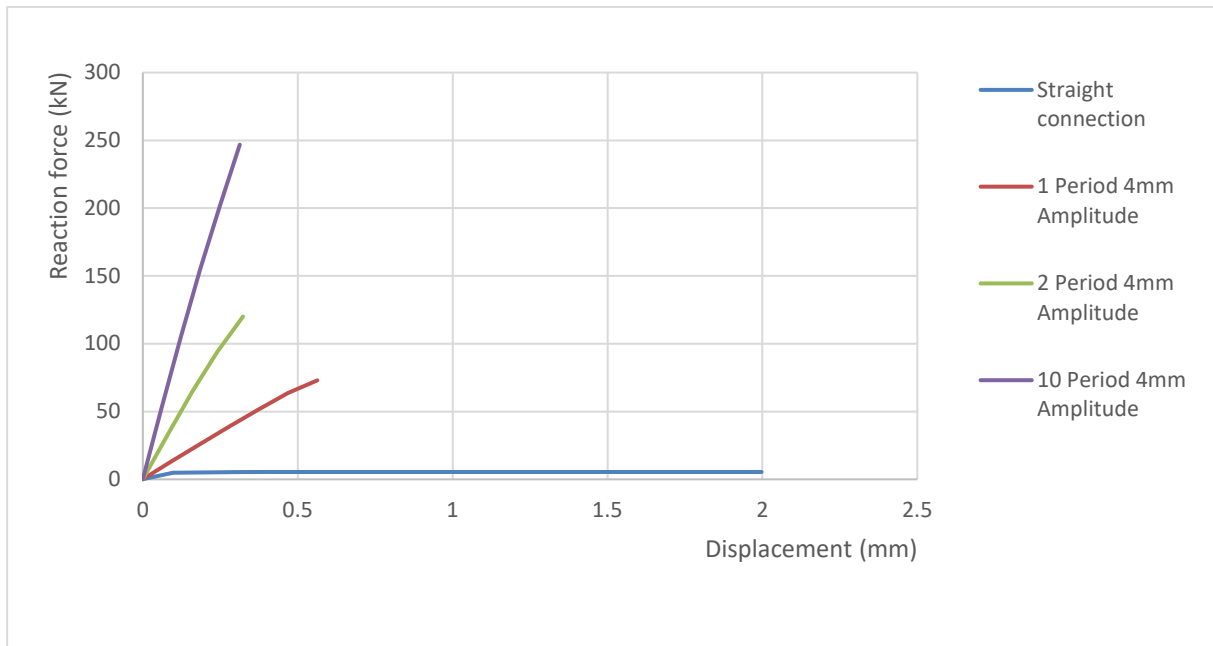
Chart 7-5: The reaction forces-displacement curve of models with different periods.
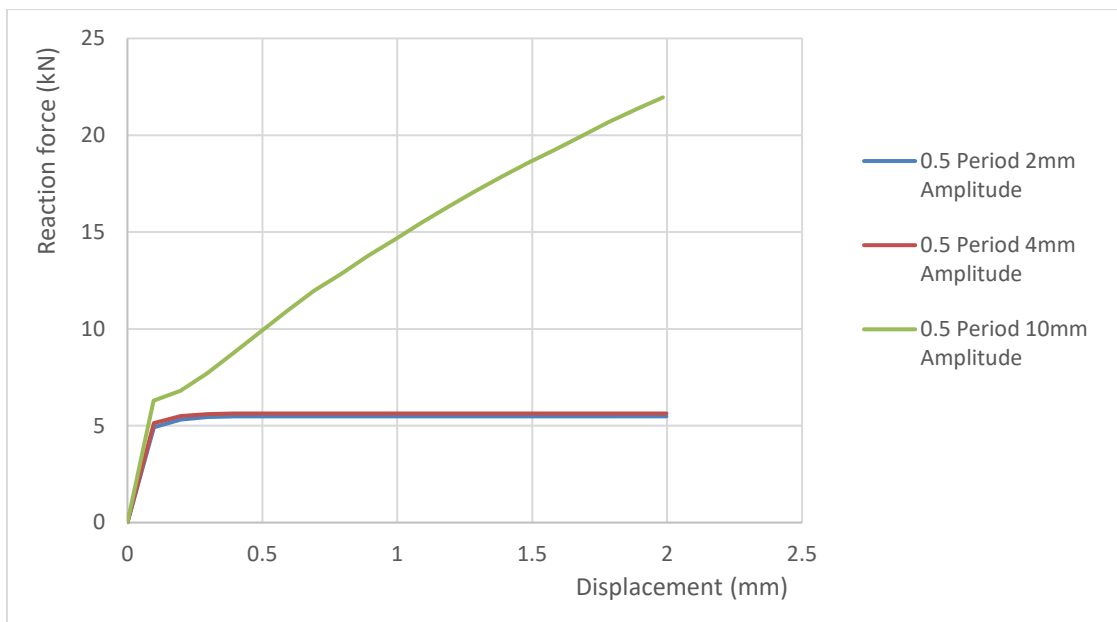
Chart 7-6: The reaction forces-displacement curve of models with half period and different amplitude.
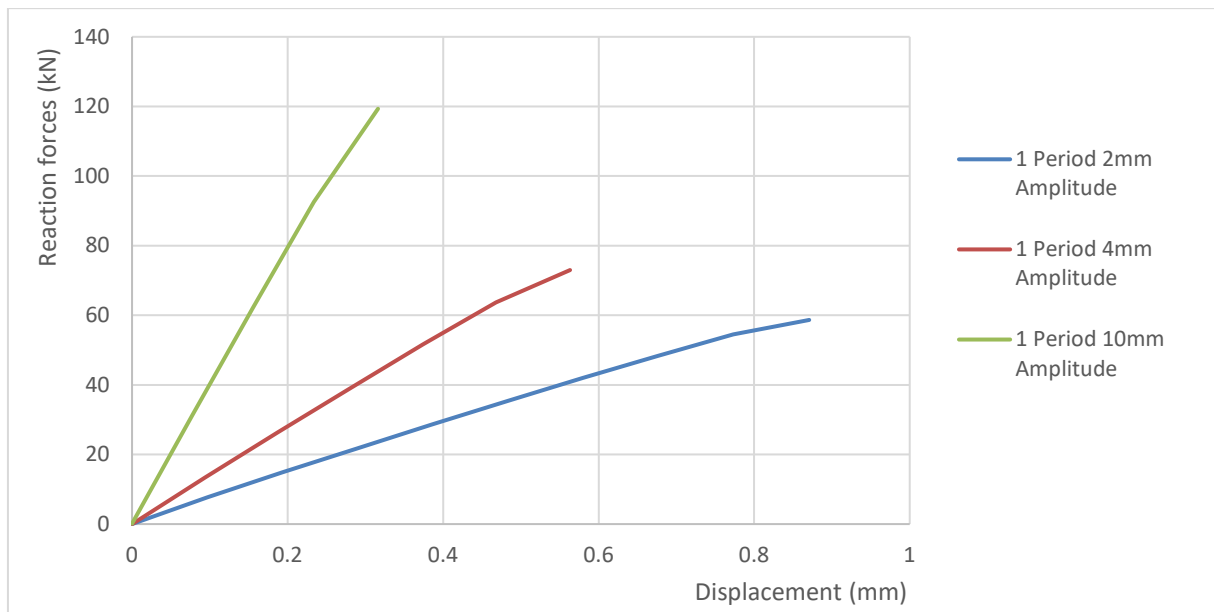
Chart 7-6: The reaction forces-displacement curve of models with 1 period and different amplitude.

Appendix F. Milling results.

Concrete age	RPM Value		
	RPM Scale 1	RPM Scale 3	RPM Scale 4
1hr after printing			
1.5hr after printing			
2hr after printing			
2.5hr after printing			

Table 7-4: The milling results with different RPM and different material status.
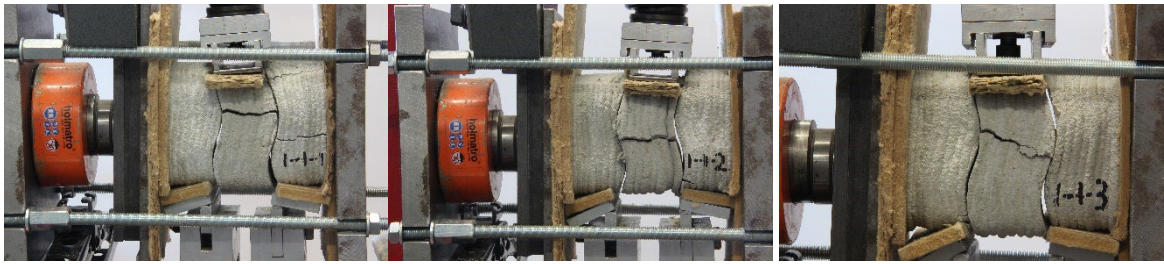
Appendix G. Experimental results of triplet shear test.

Figure 7-2: The shear test for full sine shape without interlayer material.
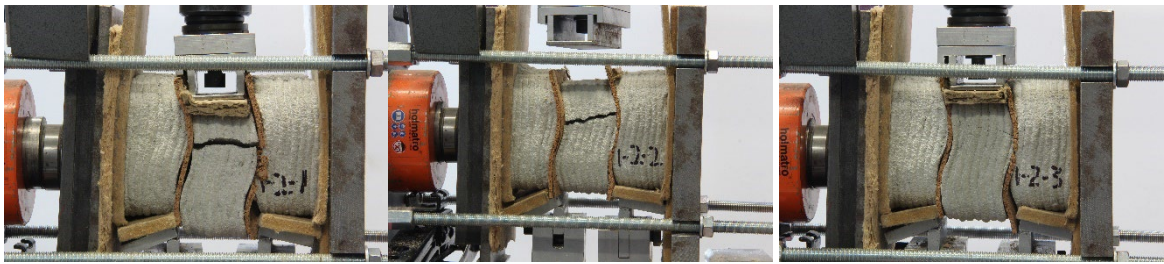

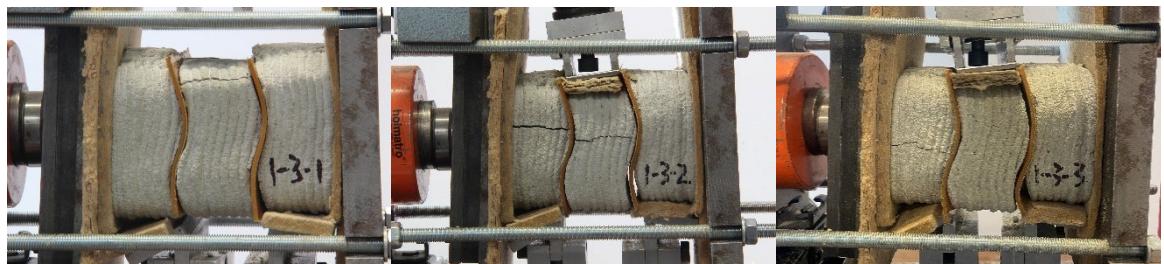*Figure 7-3: The shear test for full sine shape with cork board as interlayer material.*

Figure 7-4: The shear test for full sine shape with PU rubebr as interlayer material.

Figure 7-5: The shear test for half sine shape with cork board as interlayer material.
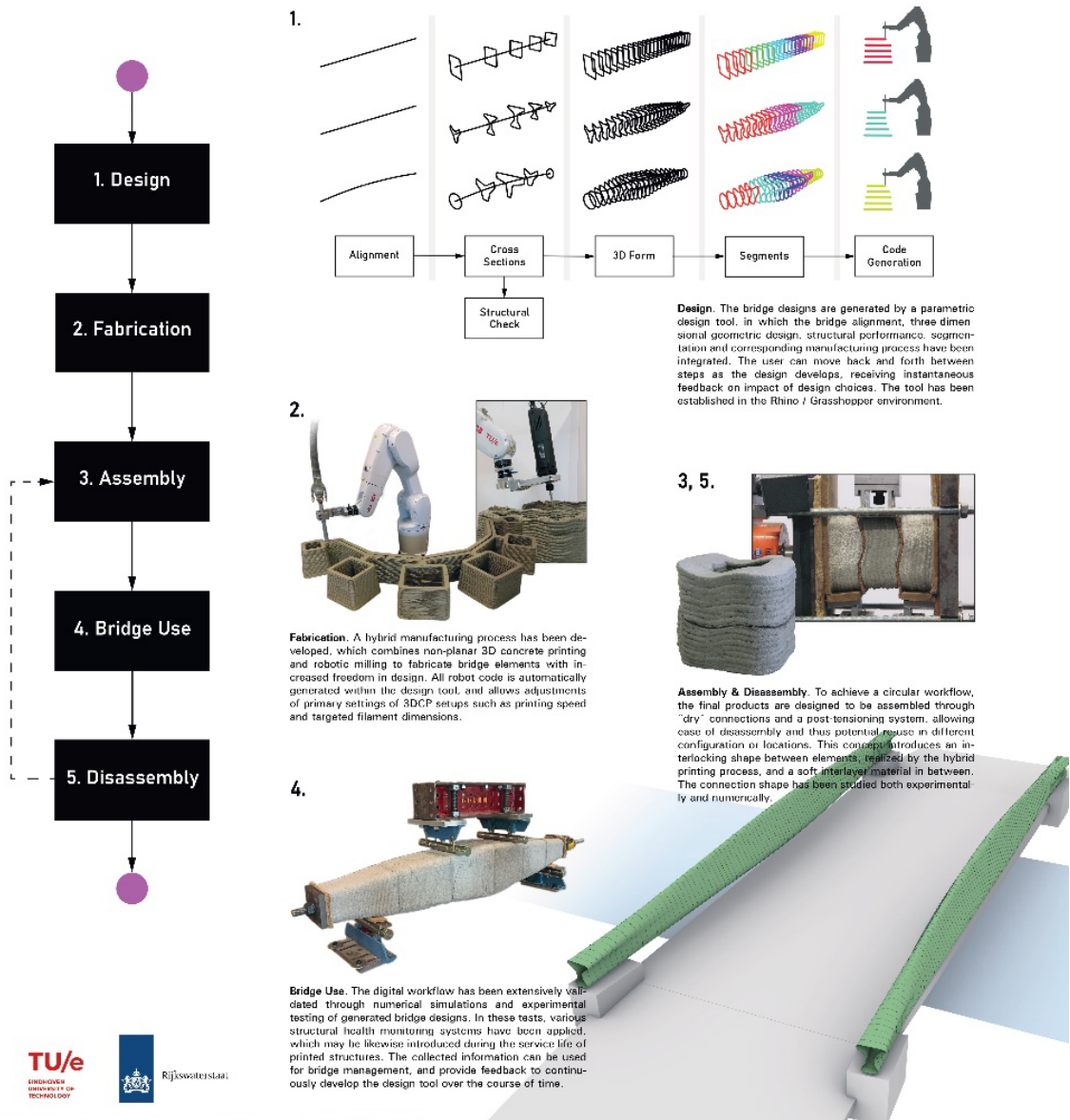

Figure 7-6: The shear test for straight connection without interlayer material.

Appendix H. Poster for Digital Concrete Conference 2022.

Figure 7-7: The poster for Digital Conference 2022.

Chapter 8. References

1. Barbosa F, Mischke J, Parsons M (2017) Improving construction productivity. https://www.mckinsey.com/capabilities/operations/our-insights/improving-construction-productivity. Accessed 17 Sep 2022

2. (2020) How construction can emerge stronger after coronavirus. https://www.mckinsey.com/capabilities/operations/our-insights/how-construction-can-emerge-stronger-after-coronavirus. Accessed 17 Sep 2022

3. Hayes M (2022) Construction skills crisis

4. United Nations Environment Programme (2019) Towards a zero-emissions, efficient and resilient buildings and construction sector. 2019 Global Status report

5. Benachio GLF, Freitas M do CD, Tavares SF (2020) Circular economy in the construction industry: A systematic literature review. J Clean Prod 260:121046. https://doi.org/10.1016/j.jclepro.2020.121046

6. Villoria Sáez P, Osmani M (2019) A diagnosis of construction and demolition waste generation and recovery practice in the European Union. J Clean Prod 241:. https://doi.org/10.1016/j.jclepro.2019.118400

7. Compendium ED, Total T (2020) Waste generation and treatment by sector , 1990-2018 Less waste being sent to landfill and more recovered. 2018–2020

8. National Waste Management Plan. https://rwsenvironment.eu/subjects/from-waste-resources/national-activities/national-waste/

9. Circular Economy. https://rwsenvironment.eu/subjects/from-waste-resources/national-activities/circular-economy/

10. Bleijenberg AN (2021) Renewal of civil infrastructure. Dutch national forecast for replacement and renovation. 1–39

11. Salet TAM, Ahmed ZY, Bos FP, Laagland HLM (2022) Design of a 3D printed concrete bridge by testing Design of a 3D printed concrete bridge by testing. Virtual Phys Prototyp 0:1–15. https://doi.org/10.1080/17452759.2018.1476064

12. Ahmed Z, Wolfs R, Bos F, Salet T (2022) A Framework for Large-Scale Structural Applications of 3D Printed Concrete: the Case of a 29 m Bridge in the Netherlands. Open Conf Proc 1:5–19. https://doi.org/10.52825/ocp.v1i.74

13. C.HARTSUIJKER, J.W.WELLEMAN (2007) Enginnering Mechanics

14. RILEM, Nicolas Roussel (2016) 276-DFC : Digital fabrication with cement-based materials

15. Wolfs RJM, Bos FP, Salet TAM (2019) Hardened properties of 3D printed concrete: The influence of process parameters on interlayer adhesion. Cem Concr Res 119:132–140. https://doi.org/10.1016/j.cemconres.2019.02.017

16. Williams A (2009) Structural Analysis

17.   VanWagnen J (2021) Element Size in FEA- Does it Matter?
       https://www.fidelisfea.com/post/element-size-in-fea-does-it-matter. Accessed 14 Sep 2022

18.   Kinnell P, Dobranski J, Xu J, et al (2021) Precision manufacture of concrete parts using
       integrated robotic 3D printing and milling. Proc 21st Int Conf Eur Soc Precis Eng
       Nanotechnology, EUSPEN 2021 57–60

19.   Oikonomopoulou F, Bristogianni T, Barou L, et al (2018) Interlocking cast glass components,
       Exploring a demountable dry-assembly structural glass system. Heron 63:103–137

20.   Anglada XR (2014) Shear tests on masonry triplets with different soft layer membranes. Swiss
       Federal Institute of Technology, Zurich, Swiss